# **Understanding Boreal Summer UTLS Water Vapor Variations in Monsoon Regions: A Lagrangian Perspective**

Hongyue Wang<sup>1</sup>, Mijeong Park<sup>2</sup>, Mengchu Tao<sup>3</sup>, Cristina Peña-Ortiz<sup>4</sup>, Nuria Pilar Plaza<sup>5</sup>, Felix Ploeger<sup>1,6</sup>, and Paul Konopka<sup>1</sup>

**Correspondence:** Paul Konopka (p.konopka@fz-juelich.de)

Abstract. Water vapor in the upper troposphere and lower stratosphere plays a crucial role in climate feedback, affecting radiation, chemistry, and atmospheric dynamics. This study presents simplified Lagrangian reconstructions of stratospheric water vapor satellite observations from SAGE III/ISS and MLS instruments, to improve the understanding of moist anomalies in the Asian and North American monsoons and to identify the key factors contributing to model biases. Our findings show that while both SAGE III/ISS and MLS capture similar spatial patterns, SAGE III/ISS shows higher local values. The performance of Lagrangian reconstructions significantly improves with the size of trajectory ensembles but exhibits a general dry bias across the tropics. However, the reconstruction represents the Asian monsoon moist anomaly well, particularly above the tropopause, whereas it fails to capture the North American monsoon anomaly. The main dehydration, region as diagnosed from trajectories, indicates that water vapor is predominantly controlled by local temperatures near the tropopause in the Asian Monsoon. North American monsoon is largely influenced by long-range transport from dehydrated regions over Southeast Asia, while moist air masses are primarily controlled by local dehydration. Hence, the limited performance of the reconstruction for the North American monsoon is potentially linked to an underestimation of local convection or uncertainty in long-range transport. Additionally, dry bias in reconstruction over the Asian monsoon shows a positive correlation with intensity of convection particularly in the western sector, suggesting that an underestimation of moistening due to convective ice injection may play a role in this region.

The

## 1 Introduction

Stratospheric water vapor (H<sub>2</sub>O) is a potent greenhouse gas that can amplify climate warming caused by emissions of well-mixed greenhouse gases in the atmosphere significantly amplify warming of the global temperature due to its strong radiative effects and long residence time (Solomon et al., 2010; Riese et al., 2012). In the tropical Upper Troposphere and Lower Stratosphere

<sup>&</sup>lt;sup>1</sup>Institute of Climate and Energy Systems, Stratosphere (ICE-4), Forschungszentrum Jülich, 52428 Jülich, Germany

<sup>&</sup>lt;sup>2</sup>U.S. National Science Foundation National Center for Atmospheric Research (NSF NCAR), Boulder, CO 80307, USA

<sup>&</sup>lt;sup>3</sup>Carbon Neutrality Research Center, Institute of Atmospheric Physics, Chinese Academy of Sciences, Beijing 100029, China

<sup>&</sup>lt;sup>4</sup>Departamento de Sistemas Físicos, Químicos y Naturales, Universidad Pablo de Olavide, 41013 Seville, Spain

<sup>&</sup>lt;sup>5</sup>Centro de Investigaciones sobre Desertificación, Consejo Superior de Investigaciones Científicas (CIDE-CSIC), 46113 Moncada, Valencia, Spain

<sup>&</sup>lt;sup>6</sup>Institute for Atmospheric and Environmental Research, University of Wuppertal, 42119 Wuppertal, Germany

(UTLS), water vapor. The amount of water vapor entering the stratosphere is primarily controlled by the strong freeze-drying process—the dehydration of moist tropospheric air entering the stratosphere at as it ascends through the cold point tropospause , a process commonly referred to as freeze-drying (Brewer, 1949; Randel and Park, 2019; Smith et al., 2021). However, the extent of hydration due to water vapor and ice directly injected. This freeze-drying occurs mainly in the tropical tropopause layer (Fueglistaler et al., 2009), where air masses ascend slowly (diabatically) from the level of main convective outflow into the 25 stratosphere through deep, overshooting convection remains uncertain (Randel et al., 2012; Avery et al., 2017; Ueyama et al., 2020; Jensen . Direct convection-driven transport involves rapid vertical updrafts near the convective center, occurring within minutes (Jorgensen and Lemone, 1989; Schwartz et al., 2013). Large-scale vertical transport enhances lower stratospheric water vapor over periods of over weeks to months and covers horizontal distances of. During this ascend, air parcels travel horizontally over thousands of kilometers (Ploeger et al., 2013), and likely sample the coldest tropopause regions (the 'cold trap') (Holton and Gettelman, 200 . A Lagrangian approach is often more suitable for assessing atmospheric conditions near the tropopause accurately as it tracks the trajectories of air parcels. In contrast, if deep convection plays a dominant role, temperature profiles below the considered point (an instantaneous perspective) may be more relevant for calculating the amount of water vapor. On the other hand, water vapor and ice can be directly injected into the lower stratosphere. Lagrangian studies reconstruct water vapor in the UTLSby identifying the coldest temperature encountered along the parcel's trajectory, often referred to as the Lagrangian CPT (Pan et al., 2018). This approach is crucial because the Lagrangian CPT reflects the long-term history of air parcels, capturing the cumulative effects of large-scale transport and temperature variability over timescales of days to even months. Several studies have successfully reconstructed UTLS water vapor using Lagrangian methods that track the minimum saturation mixing ratio of air parcels based on the Lagrangian CPT (Mote et al., 1995; Fueglistaler and Haynes, 2005; Liu et al., 2010; Schoeberl and Dessler . This perspective highlights the importance of considering the history of air parcels in understanding the Upper Troposphere and Lower Stratosphere (UTLS) through deep, overshooting convection, and it has been argued that this process happens frequently in the tropics and over North America during boreal summer (Homeyer et al., 2023). This convection-driven transport is characterized by rapid vertical updrafts near convective centers, occurring in the timescales on the order of minutes (Jorgensen and Lemon . However, the extent to which this hydration process affects stratospheric water vapor distribution remains under debate

During boreal summer, enhanced UTLS water vapor mixing ratios are water vapor is observed in the UTLS over regions influenced by the Asian Summer Monsoon (ASM) and the North American Monsoon (NAM), both of which experience intense convection (Fu et al., 2006; Yu et al., 2020; Park et al., 2021; Clemens et al., 2022). (Ploeger et al., 2013; Park et al., 2021; Clemens et al., 2022). (This enhancement is often attributed to intense convection, which can transport water vapor directly into the UTLS (Fu et al., 2006; Yu et al., 2006

(Randel et al., 2012; Avery et al., 2017; Ueyama et al., 2020; Jensen et al., 2020; Ueyama et al., 2023; Homeyer et al., 2023; Konopka et al.

been recognized as a major contributor to stratospheric water vapor (e.g. Bannister et al., 2004; Wright and Gille, 2011; Rolf et al., 2018)
, with this contribution amounting to about, accounting for ~15% of the tape recorder anomaly maximum in the tropical lower stratosphere and to about tropical stratospheric water vapor anomaly and ~30% of the summertime maximum in the NH extratropical lowermost stratosphere (Nützel et al., 2019)NH extratropical water vapor maximum (Bannister et al., 2004; Wright and Gille, . These observational studies, however, have limitations in understanding the physical processes that are driving the enhancement in water vapor concentrations over the monsoon regions. Understanding those mechanisms and the interactions between regional convection, large-scale transport and thermodynamic conditions is the key to predict the potential impact of stratospheric water vapor on our climate.

In this study, we aim to further investigate the physical processes responsible for the enhanced our goal is to evaluate the role of the freeze-drying mechanism in the large-scale temperature and wind fields for the enhancement of stratospheric water vapor over the ASM and NAM regions . To achieve this, we from a Lagrangian perspective. Lagrangian methods track the history of air parcels (their trajectories) and reconstruct stratospheric water vapor based on the coldest temperature encountered along these trajectories, commonly referred to as the Lagrangian cold points (LCP) temperature (Fueglistaler et al., 2005). By capturing the cumulative effects of large-scale transport and temperature variability over timescales ranging from days to months, Lagrangian methods have been successfully used to reproduce UTLS water vapor anomalies (Mote et al., 1995; Fueglistaler and Ha . We firstly conduct Lagrangian back-trajectory simulations utilizing the trajectory module of the Chemical Lagrangian Model of the Stratosphere (CLaMS) (McKenna et al., 2002), to reconstruct satellite observations by the Stratospheric Aerosol and Gas Experiment III on the International Space Station (SAGE III/ISS) Davis et al. (2021) Version 5.3 and Aura Microwave Limb Sounder (MLS) Version 5.0 Lambert et al. (2017). These Lagrangian reconstructions are driven by the fifth generation European Centre for Medium-Range Weather Forecasts atmospheric reanalysis (ERA5) (Hersbach et al., 2020). We then assess the performance of the Lagrangian reconstruction in capturing boreal summer UTLS water vapor distributions by comparing simulation results with satellite datasets from SAGE III/ISS (Stratospheric Aerosol and Gas Experiment III on the International Space Station) and MLS (Aura Microwave Limb Sounder). This analysis also involves contrasting the summer monsoon regions with the entire to the satellite observations. Additionally, we compare the monsoon regions to the deep tropics, where convection is less dominant similar Lagrangian reconstructions were successfully applied in the past 80 (Fueglistaler et al., 2005; Hasebe and Noguchi, 2016; Smith et al., 2021). We utilize SAGE III/ISS is utilized for its higher vertical resolution (2 km compared to ~3 km in MLS near the UTLS region (Read et al., 2007)), which provides providing a more detailed representation of H<sub>2</sub>O water vapor vertical structures within the monsoon anticyclones. The MLS dataset is used for comparison due to its extensive sampling coverage and widespread application. MLS provides daily global coverage and has widely been used in numerous studies on stratospheric water vapor Mote et al. (1995); Liu et al. (2010); Nützel et al. (2019) . Furthermore, we discuss analyze the spatial and temporal locations of the Lagrangian cold points LCPs in relation to the observed water vapor in distributions within the monsoon regions. We also identify processes that may explain differences We also investigate the potential factors contributing to discrepancies between the Lagrangian reconstruction and observed data reconstructions and observations, with a primary particular focus on deep convection, which is not fully only partly resolved in ERA5 meteorology but can be quantified using. As a proxy for the intensity of convection, we use Outgoing Longwave Radiation (OLR) derived from satellite observations (Kumar and Krishnan, 2005).

The main research questions explored in this paper are: (i) How well can stratospheric water vapor mixing ratios in the ASM and NAM as observed by SAGE III/ISS and MLS be reconstructed using Lagrangian methods simplified Lagrangian modelling method, especially in comparison to the tropics where such methods were successfully applied in the past (Fueglistaler et al., 200 deep tropics? (ii) Are the moisture anomalies observed within the ASM and NAM anticyclones locally or remotely controlled by the Lagrangian CPT LCPs and which regions are most critical? (iii) Does the Lagrangian reconstruction support the finding that "stronger convection leads to a relatively dry stratosphere (and vice versa)" as found by Randel et al. (2015) Are model biases in the reconstruction related to particular processes (e.g., convection)?

This paper is organized as follows: Section 2 presents the datasets and model used, and describes the reconstruction method.

Section 3 outlines our main results, including the assessment of Lagrangian water vapor reconstructions concerning both horizontal and vertical aspects, and the analysis of Lagrangian cold points LCPs. Section 4 discusses the potential causes of biases in the Lagrangian reconstruction results and relations to convection. Section 5 provides the conclusions.

## 2 Data and Method

## 2.1 Satellite observations

#### 105 2.1.1 MLS

110

120

The Microwave Limb Sounder (MLS) instrument on the Aura spacecraft satellite Waters et al. (2006) has been providing global measurements of various atmospheric constituents since August 2004, including water vapor, ozone, carbon monoxide, sulfur dioxide, nitric acid, and nitrous oxide profiles using radiances from the nearest limb scan (https://www.earthdata.nasa.gov/learn/find-data/near-real-time/mls). MLS provides a comparatively high sampling with about 3500 measurement profiles per day. Here, we use version 5.0 (v5.0) data, which provides water vapor profiles in 2.1-3.5 3.5 km vertical resolution (Lambert et al., 2017), with ~3.0 km resolution in lower stratosphere (Read et al., 2007). We focus on water vapor profiles in measurements for the month of August from 2017 to 2019 across the tropics. Binned data for horizontal distributions are gridded with resolution of in the subtropical regions (35°S-35°N). The MLS water vapor profiles are then gridded in 10°× 20°(latitude × longitude) horizontal grids. For more details on MLS water vapor and the retrieval technique see Read et al. (2007)Livesey et al. (2020).

#### 2.1.2 SAGE III/ISS

The Stratospheric Aerosol and Gas Experiment III on the International Space Station (SAGE III/ISS) — was launched on February 19, 2017 Cisewski et al. (2014) and has been providing measurements of aerosol, water vapor and ozone between 70°S and 70°N latitude using solar occultation, lunar occultation and limb scattering. We use Level 2 (L2) Solar Event Species Profiles (HDF5) Version 5.3 (v5.3) data product () contains comprehensive profiles of key atmospheric components

eollected during solar occultation events. SAGE IIIhttps:/ISS, launched on February 19, 2017, employs techniques such as solar occultation, lunar occultation, and limb scattering to measure acrosols, ozone, water vapor, and other trace gases across latitudes from 70°S to 70°N./asdc.larc.nasa.gov/project/SAGEAccording to Davis et al. (2021), there is generally good agreement between SAGE III/ISS v5.1 and MLS v5.0 in stratospheric water vapor measurements in the stratosphere, with SAGE III/ISS v5.1 values being approximately being drier than MLS (~0.5 ppmv (or 10%) drier than MLS over the 15–35 in the 15–35 km altitude range. However, SAGE III/ISS v5.1 profiles were affected by low-quality data due to aerosol and cloud-related interferences (Park et al., 2021; Davis et al., 2021). These issues—such as failed retrievals and increased sensitivity to elevated aerosol loading—were largely mitigated in version 5.2 and subsequent versions, as noted in the SAGE III/ISS Data Products User's Guide (https://asdc.larc.nasa.gov/documents/sageiii-iss/guide/DPUG\_G3B\_v05.30.pdf).

We focus on data in August from 2017 to 2022, using v5.3 of the water vapor profiles within the entire tropies measurements in the month of August for 2017-2022 in the subtropics (35°S to 35S-35°N). In addition to the years covered by MLS (2017-2019), we include We added three more years to enhance statistical robustness for (2020-2022) of the SAGE III/ISS measurements to increase spatial coverage of SAGE III/ISS , as the water vapor. Comparison of the horizontal distributions of SAGE III/ISS dataset has lower horizontal and temporal samplingwater vapor for the 2017-2019 and 2017-2022 periods results in no significant differences and does not affect the results of our study. The water vapor profiles provided by SAGE III/ISS v5.3 product are originally retrieved on a 1.0 km grid and interpolated on a 0.5 km grid from 0.5-60.0-60.0 km in altitude. In this study, we perform a 1-2-1 vertically vertical smoothing on all SAGE III/ISS water vapor profiles on a 0.5 km grid following Davis et al. (2021), resulting in a final vertical resolution of 2 km. The profiles are presented in units of number density. We convert the units into mixing ratio using temperature and pressure profiles from the Modern-Era Retrospective analysis for Research and Applications, Version 2 (MERRA-2). Binned data used here for presenting horizontal distributions are gridded with resolution of 10°× 20°(latitude × longitude), requiring at least 5 profiles in each bin. We follow the similar procedure described in Park et al. (2021), where SAGE III/ISS v5.1 was used.

#### 2.2 OLR

130

135

140

150

For representing the strength of convection, we utilize daily mean Outgoing Longwave Radiation-We use daily mean outgoing longwave radiation (OLR) data as a proxy for deep convection. The OLR data is obtained from the National Oceanic and Atmospheric Administration (NOAA) Climate Prediction Center (CPC) (https://psl.noaa.gov/data/gridded/data.cpc\_blended\_olr-2.5deg.html). The CPC blended OLR Version 1 dataset is constructed by blending the level 2 OLR retrievals from NASA's Cloud and Earth Radiant Energy System broadband measurements, NOAA/NESDIS Hyperspectral measurements, and High-resolution Infrared Radiation Sounder measurements. The dataset provide daily OLR values gridded daily OLR from NOAA covers the period from 1991 /01/01 to the most recent available date, on a 2.5°× 2.5° (latitude × longitude) global grid. We substract the monthly average subtract the monthly averages at each grid point to obtain the OLR anomalies. The OLR indices used in this study are calculated by averaging the OLR anomalies within specific regions. The regions For the ASM, the indices are defined as follows: (i) OLR-West: 20-3020-30°N, 50-8050-80°E, (ii) OLR-East: 20-3020-30°N, 80-11080-110°E. Here the indices are defined only for the ASM. This separation of convective regions in the ASM follows Randel et al. (2015), and

our results are not sensitive to the exact separation longitude. For the OLR values shown in Fig. 8, we use the original values instead of anomalies. Note that, while OLR is a commonly used proxy for convective intensity, it has limitations in identifying deep convection due to its reliance on infrared measurements. These measurements can misinterpret underestimate cloud-top temperatures, particularly over land and for aged anvil clouds (Liu et al., 2007).

## 2.3 Models

165

175

180

## 160 2.3.1 CLaMS trajectory module

Chemical Lagrangian Model of the Stratosphere (CLaMS) is an advanced modeling framework designed for simulating the transport and chemical processes in the atmosphere (McKenna et al., 2002; Konopka et al., 2022). It employs a Lagrangian approach, where air parcels are tracked individually, allowing for a detailed and accurate representation of atmospheric dynamics and chemistry. For this study, we use the trajectory module of CLaMS 2.0, which specifically focuses on the trajectory calculations of air parcels (https://clams.icg.kfa-juelich.de/CLaMS/traj). The driving meteorological fields for these simulations are from ERA5, with 1°× 1° (latitude × longitude) horizontal resolution, 137 vertical hybrid layers and 6-hour time interval (Hersbach et al., 2020). We perform 180-day back-trajectory calculations for air parcels, with each air parcel launched from the precise spatial location and time corresponding to the satellite data profiles within ASM and NAM. For the the tropics. For each August from 2017 to 2022, SAGE III/ISS dataset, we set the starting points at altitudes ranging from 14.0 km to 21.0 km, with a 0.5 km interval, matching the vertical resolution of the SAGE III/ISS profiles. For the MLS dataset, we determine the starting points by identifying the corresponding geopotential height for each layer in the MLS profiles, ensuring they are set accordingly. In both cases, the trajectories are initialized at the exact horizontal location and time of provides 149, 203, and 2292 profiles for the ASM, NAM, and tropics, respectively. For each August from 2017 to 2019, MLS provides 7801, 10,223, and 126,981 profiles for the ASM, NAM, and tropics, respectively. Taking the ASM as an example, the satellite measurements, aligning the calculations closely with the observational data. number of calculated trajectories is determined by  $149 \times 10$ (profiles × levels) for the LAG single experiment (for the definition of the different model experiments see Sect. 2.3.2) and  $149 \times 10 \times 51$  (profiles × levels × ensemble trajectories) for the LAG experiment. Accordingly, the total number of calculated trajectories for LAG\_single is 1490 for the ASM, 2030 for the NAM, and 22,920 for the tropics, while for LAG, these values increase to 75,990, 103,530, and 1,168,920, respectively. Similarly, for MLS the number of trajectories for LAG single is 39 005 for the ASM, 51 115 for the NAM, and 634 905 for the entire deep tropics, while for the LAG experiment these values are multiplied by 51, resulting in significantly larger trajectory ensembles.

#### 2.3.2 Water vapor reconstruction

We reconstruct water vapor concentrations by identifying the CPTcold point temperature. From the local perspective, cold points are the lowest temperatures observed along local vertical profiles. From the Lagrangian perspective, the cold points are defined as the minimum temperatures encountered along the back-trajectories of air parcels, after interpolating the ERA5 temperature and pressure data along the back-trajectories. The reconstructed stratospheric water vapor concentrations are cal-

culated using the following formulas:  $H_2O_{\text{ppmv}} = 1.0 \times 10^6 \cdot e_{\text{sat}}/(P - e_{\text{sat}})$ , where the saturation vapor pressure  $e_{\text{sat}}$  is given by  $e_{\text{sat}} = 10^{\left(\frac{A}{CPT} + B\right)}/100$ . Here, A = -2663.5, B = 12.537, CPT is the <u>cold point</u> temperature in K, and P is the pressure in hPa (Sonntag. 1994).

190 In the following, we present the results of three results from our experiments based on three types of reconstructions: LOC, LAG single and LAG. (a) LOC uses the minimum temperatures along the local temperature profiles, i.e., the local CPTs. to calculate the reconstructions. On the other hand, LAG single and LAG both use the Lagrangian CPTs-vertical profiles associated with SAGE III/ISS, which are derived from MERRA-2 reanalysis. These minimum values are treated as local cold point temperatures (CPTs) and are used in the previously introduced equations to calculate the reconstructions, but they employ different methods for identifying the CPTs... (b) For LAG single, we initiate back-trajectoy simulation from every single 195 satellite observation-back-trajectory simulations are initialized on each measurement point in the UTLS, using the observed altitude, longitude, and latitude of that point. For LAG, we reconstruct Upon obtaining the trajectories, we then find the LCP temperatures to calculate the reconstructions at all the observation points. For the SAGE III/ISS dataset, we set the starting points at altitudes ranging from 14.0 km to 21.0 km, with a 0.5 km interval. For the MLS dataset, we convert pressure to geopotential height then used the one closest to the SAGE III/ISS altitude. (c) For LAG, each measurement point from an 200 is reconstructed using an even larger ensemble of trajectories by adding initiating 50 additional starting points around each observation point, spaced 10 meters vertically vertically spaced at 10-meter intervals above and below the observation point. and then consider the ensembles of. This results in a total of 51 trajectories, including the original one at the observation point. The reconstruction is then based on the ensemble of these back-trajectories. For example, if the observation point is at 16.0 km 205 (as in the SAGE III/ISS dataset), we set the starting point at 16.0 km and add 50 more points from 15.25 km to 16.25 km, with 0.01 km (10 meters) intervals intervals. The final reconstruction value for this observation point is calculated by averaging the reconstruction values from all 51 back-trajectories, to enhance the vertical sampling around the original observation point. We focus on increasing the sampling in the vertical direction rather than the horizontal. The final reconstruction value is obtained by averaging all the reconstructed back-trajectories. This dense sampling enhances the vertical resolution of the reconstruction. We specifically increase vertical sampling because vertical wind shear in the atmosphere tends to redistribute air horizontally. 210 Over time, air parcels stretch into thin, wide layers, similar to pancake-like structures, as a result of generally leads to stronger redistribution of air parcels compared to horizontal shear. As air parcels move, they are stretched into thin and horizontally extended layers due to quasi-isentropic flow. This natural horizontal spreading reduces the need for more horizontal sampling, as parcels dilute gradually through stirring. Additionally horizontal spreading gradually dilutes the parcels and lessens the necessity for denser horizontal sampling. Also, given the vertical resolution of MLS and SAGE III/ISS data (3 km and 2 km, 215 respectively), it is more important to increase the vertical sampling in our trajectory calculations to better reconstruct the water vapor mixing ratios. For further details on this process, we of these processes, refer to Haynes and Anglade (1997), which explains how differential advection in the atmosphere drives vertical mixing and stretching of air parcels.

All the back-trajectories are categorized into two groups: those that cross the tropopause , which represent are referred to as Troposphere-to-Stratosphere Transport (TST), and those that do not , are referred to as non-TST. TST trajectories are defined as those with starting points (or observation points) located above 370 K potential temperature and traceable traced back to

below 340 K potential temperature. For TST trajectories, the reconstructed water vapor concentrations are calculated using the Lagrangian CPTsLCP temperatures. For non-TST trajectories, the reconstruction reconstructed values are defined as the smaller values between the saturation values, calculated using Lagrangian CPTs of the two: the saturation mixing ratios based on LCP temperatures, and the zonal monthly climatological water vapor concentrations (MLS) at the from MLS at the earliest back-trajectory endpoints (the earliest points in time).

## 3 Results

225

245

250

## 3.1 Performance of Lagrangian water vapor reconstruction

## 3.1.1 Spatial distributions

In boreal summer, both Both the ASM and NAM regions feature high water vapor concentrations within the UTLS show 230 enhanced water vapor mixing ratios based on satellite observations during boreal summer. Figure Figures 1a and 1b present the horizontal distribution show horizontal distributions of water vapor in August at ~16.5 km (around 100 hPa and pressure level or 380 K potential temperature level) based on SAGE III/ISS and MLS satellite observations, respectively. The distributions from both satellite datasets show consistent spatial patterns, with notably high water vapor concentrations located in 235 the two main monsoon regions, the maxima located over the ASM (15°-35-35°N, 50°-150-150°E) and NAM (10°-35-35°N, 160°-80-80°W). The high values from SAGE III/ISS (exceeding 7 ppmv) are higher than the values from MLS (5-6-5-6 ppmv). Figure 1e-d show c and 1d present reconstructed water vapor from Experiment LAG with derived from ensemble trajectories (Experiment LAG), where more than 80% TST trajectories of the trajectories are classified as TST (Sect. 2.3.2), based on the profiles from SAGE III/ISS and MLS, respectively. The large-scale patterns in the reconstructions are consistent with the observations, but there are obvious dry biases throughout the entire tropics, especially in the NAM region. Overall, 240 the reconstructions exhibit a noticeable dry bias across the entire tropics compared to the observations. Concerning the spatial patterns, however, the water vapor distributions reconstructed from trajectories for the two satellite datasets are similar, in particular showing elevated mixing ratios above the ASM, similar as in the satellite observations. While the elevated water vapor mixing ratios in the ASM are captured, the observed moist anomaly in the NAM is not reconstructed from trajectories.

The anomalies shown in Fig. 1e-h are derived by subtracting the average values of the entire tropics. The observed anomalies from SAGE III/ISS in are ~1–2 ppmv over the ASM and NAM (Fig. 1eillustrate that during monsoon season, water vapor concentrations in the ASM and NAM increase by 1–2 ppmv, while from MLS (), which is higher than the those from the MLS (~1 ppmv) as shown in Fig. 1f), the increases are slightly smaller, amounting to approximately 1 ppmv. Comparing the anomalies of both reconstruction and observationCompared to the observations, the reconstruction captures the enhancements in water vapor concentrations and their locations, particularly in the ASM region, where the elevation of water vapor (1-2 ppmv) is nearly fully reproduced, though with slightly more limited coverage successfully captures the water vapor anomalies over the ASM (1–2 ppmv), covering smaller area. However, the reconstruction performs unsatisfactorily in the NAM region,

with over the NAM shows an increase of less than 0.5 ppmv being reproduced in water vapor concentrations, with the maximum located near the equator.

255 Figure 2 analyzes the vertical structure of the observed and reconstructed water vapor profiles, averaged over the three regions of interest; tropics, ASM, and NAM. As expected, all water vapor values along the profiles increase from the stratosphere All water vapor profiles show a decrease in concentration from the troposphere to the UTLS region, and the. The variability in water vapor is greater in the troposphere than in the stratosphere. The reconstructed profiles partially reproduce the observed enhancements in both water vapor concentrations and variations capture these distinct characteristics of water vapor in both the troposphere and stratosphere, in terms of both concentration and variability. The reconstructed profiles exhibit

260

265

280

285

In the tropics (Fig. 2a-b), the cold point tropopause and the lapse rate tropopause are located at 16.7 km (cvan dashed lines) and 15.7 km (yellow dashed lines), respectively. Below the lapse rate tropopause, the reconstructed profiles (blue lines) based on SAGE III/ISS show maximum dry biases of up to 5 ppmv in the upper troposphere below 16 km. At 16.5 km, in the UTLS-2.3  $\pm$  2.5 ppmv at 15.5 km, while MLS-based reconstructions exhibit biases of -1.5  $\pm$  1.5 ppmv at ~15.1 km. Within the tropical tropopause layer (between the cold point and lapse rate tropopauses), both the magnitude and variability of the dry biases gradually decrease with increasing altitude. Above the cold point tropopause, the dry biases are 2-3 ppmy decrease to  $-1.7 \pm 0.7$  ppmy (-34%  $\pm 14$ %) at 17.0 km based on SAGE III/ISS, and to -0.8  $\pm 0.6$  ppmy (-21%  $\pm 15$ %) at ~17.4 km based on MLS. Similar dry biases are have been reported by Liu et al. (2010), who found that stratospheric water vapor predictions for the stratospheric overworld based on the saturation mixing ratio at the Lagrangian dry point of trajectories exhibit dry biases of up to  $-50-50\% \pm 10\%$ , which they attributed to missing cloud microphysics. Above 19.0 km, the biases in the reconstructions are 1-2-1-2 ppmv smaller when both TST and non-TST trajectories are considered (Fig. 2S1), compared to when only TST trajectories are used (Fig. \$\frac{1}{2}\$). The evan squares black diamonds in Fig. \$1 represent the percentage of TST trajectories relative to the total number of trajectories, indicating that non-TST trajectories account for more than 95% above 19.0 km. This suggests that water vapor concentrations in the higher stratosphere align more closely with climatological values and less with direct transport from the upper troposphere within 180 days.

For In monsoon regions, the main structures of both observed and reconstructed profiles are similar to those in the tropics. though there are some noticeable differences. From the observed profiles, UTLS water vapor concentrations in monsoon regions are 2-4 ppmy higher than in the entire tropics. The enhancements of water vapor in the ASM from SAGE III/ISS, especially below the lapse rate tropopause. The anomalies of observations, compared to the average in the tropics, reach 4.5 ppmy at 16.5 km for the ASM (Fig. 2c) are the most significant, exceeding 4 ppmv at 15.5 km. For the reconstructions, compared to the profiles and 1.5 ppmv for the NAM (Fig. 2c), as derived from SAGE III/ISS observations.

In the ASM region, the tropopause layer is higher and thinner (16.6–17.1 km) compared to that in the tropics. For the reconstructions based on SAGE III/ISS, the reconstructed profiles in ASM profiles have substantial dry biases below the lapse rate tropopause, up to  $-4.9 \pm 4.2$  ppmv at 15.5 km (Fig. 2c-d). However, these biases gradually decrease with altitude, reducing to  $-1.7 \pm 0.8$  ppmv at 17.5 km, consistent with the bias levels seen in the tropics. To further assess the vertical performance of the reconstruction, we compare the reconstructed ASM anomalies relative to the entire tropics. At 15.5 km, the SAGE-based reconstructions capture approximately one-third of the ASM capture an increase of ~1 ppmy in the UTLS observed anomalies (Fig. 2e-d), and the dry biases increase to 2-5 ppmv.—2b; right sub-panels). The agreement improves significantly with altitude: at 16.5 km, the reconstructed anomalies account for over two-thirds of the observed values, and above this level, the reconstructions approach even closer agreement. Similar results are also reflected in the MLS-based reconstructions (Fig. 2e; right sub-panels). This shows that the Lagrangian reconstruction method performs reliably above tropopause levels. The consistent behaviour of the reconstruction in the ASM compared to the tropics further suggests that stratospheric water vapor above the ASM is primarily governed by the mechanisms-freeze-drying in the large-scale temperature field ('advection-condensation' paradigm, see Liu et al., 2010)—as in the tropics. In contrast, at lower altitudes in the troposphere, water vapor is likely more strongly influenced by other processes such as deep convection. Consistent with our findings, Plaza et al. (2021) showed that while convection can moisten the upper troposphere, its signature could be erased by subsequent dehydration at higher altitudes. As a result, convection plays a limited role in determining water vapor concentrations in the lower stratosphere of monsoon regions, whereas small-scale mixing appears to be a more dominant contributor.

In the NAM, the reconstructed profiles show insignificant differences compared to those tropopause layer (15.6–16.5 km) is slightly lower and thinner compared to that in the tropics (Fig. 2e-f), with biases of 3-4 ppmv...c and 2f). As the altitude increases, the bias profile based on SAGE III/ISS decreases more slowly than in the ASM, with a remaining bias of -1.8 ± 1.2 ppmv at 17.0 km within the stratosphere (Fig. 2c). Moreover, the fraction of the observed anomaly captured by the reconstruction is considerably lower in the NAM compared to both the ASM and the tropics (Fig. 2c and 2f; right sub-panels). The distinct structure of the tropopause layer and the corresponding reconstruction performance in the NAM suggest that considering only the freeze-drying effect by advection through the large-scale temperature field (as represented in the Lagrangian reconstruction method) is insufficient to explain the moist anomaly in the NAM region. Hence, further processes like convection, mixing, and ice microphysics are likely to play a more significant role in stratospheric water vapor variability in the NAM.

Comparing the profiles from SAGE III/ISS (left) with those from MLS (right), the higher vertical resolution profiles from SAGE III/ISS show more strongly enhanced water vapor concentrations and clearer peak values in the UTLS for the entire tropics, including the monsoon regions, especially in three regions of focus, especially the ASM. Additionally, the The reconstructions based on SAGE III/ISS and MLS resemble each other, both capturing an enhancement of ~1 ppmv of water vapor in the ASM but not in the NAM.

. The SAGE III/ISS dataset, with its higher vertical resolutioncompared to MLS, captures more features of water vapor variations in the UTLS, while MLS may lose information due to its coarser layerslower vertical resolution. However, the limited and uneven sampling of SAGE III/ISS might restrict its ability to reveal spatial features, which could also be the main reason for the slight differences between the reconstructions based on the two datasets. The diagnosed dry biases in the reconstructed water vapor concentrations could be due to systematic temperature differences in the ERA5 reanalysis (Tegtmeier et al., 2020), but are probably mainly attributable to moistening processes not included in the trajectory simulations, such as deep convection and related ice injection. Nonetheless, the analysis above implies that the reconstruction using Lagrangian CPT generally reproduces the overall horizontal patterns and vertical structures across the tropics and within the ASM, but it does not adequately capture the patterns in the NAM.

## 3.1.2 Lagrangian versus local reconstruction sensitivities

335

340

345

350

355

To assess the performance of the reconstructions from different experiments, we present the correlation coefficients between observed and reconstructed water vapor concentrations in Fig. 3. The x-axis in each plot shows the length of the backward period used for the trajectory calculations. In addition to LAG the Lagrangian reconstruction using cold point temperatures from ensemble trajectories (LAG) based on both SAGE III/ISS and MLS datasets, we include also include the reconstruction using cold point temperatures from individual trajectories (LAG\_singleand LOC) and the reconstruction using local cold point temperatures (LOC) only based on SAGE III/ISS to compare local and Lagrangian methods profiles. This allows a direct comparison of the Lagrangian methods with the local perspective. Note that the x-axis in each plot shows the length of the backward period used for the trajectory calculations, thus the correlation coefficients for LOC remain constant.

The reconstructions from LAG exhibit the highest correlation with observations, followed by LAG single, while LOC shows the lowest correlation coefficients: -0.12 in the tropics, 0.07 in the ASM, and -0.17 in the NAM, indicating that it is not the. As expected, using local cold point that determines water vapor concentrations, neither in the deep tropics (as e.g. shown by Fueglistaler et al., 2005) nor in the summertime monsoon regions. Furthermore, the simulation with higher resolution (LAG) demonstrates significantly better performance measured as higher correlation, compared to the simulation with lower resolution temperatures to determine stratospheric water vapor yields unreliable results (compare Fueglistaler et al., 2005) . Similarly, smaller trajectory ensembles (LAG single) . This is because LAG single relies on individual trajectories, which have limited accuracy, as trajectory reconstructions are highly sensitive to the initial position of the air parcel air parcel position and small variations in the ERA5 wind and diabatic heating fields. As a result, the uncertainty in the parcel's position increases as the trajectory is traced backward. On the other hand, LAG uses trajectory ensembles, which account for uncertainties in the initial conditions and slight differences in the ERA5 fields. By averaging over these ensembles larger trajectory ensembles (LAG), the reconstruction becomes more robust and accurate, as it better captures the uncertainties inherent effectively capturing the inherent uncertainties in the system. For LAG the results based on MLS and SAGE III/ISS, changing the dataset does not significantly affect reconstruction performance across the three regions. This suggests that the results based on SAGE III/ISS are generally representative and reliable for the objectives purposes of this study, despite its less lower horizontal and temporal sampling compared to MLS. Moreover, the comparison across the three regions shows no significant distinctions, indicating that the efficiency of the Lagrangian reconstruction does not vary noticeably between monsoon regions and the entire tropics.

The reconstruction of water vapor using the Lagrangian method aims to find the minimum saturation mixing ratio along the trajectory, and therefore the backward time length of the simulation might influence the results. As shown in Fig. 3, all Lagrangian experiments display a consistent increasing trend in correlation coefficients as the backward calculation time increases. For instance, in LAG (SAGE III/ISS), the correlation coefficients for the ASM region increase from 0.53 (with a 60-day backward period) to 0.69 (with a 180-day backward period), and from 0.43 to 0.75 for the NAM. The most rapid increase occurs when extending the backward period from 60 to 120 days. These significant improvements in the reconstruction suggest that UTLS water vapor concentrations in August are partially influenced by processes from boreal spring or even winter, with

a potentially stronger influence particularly at higher altitudes, as air parcels at those levels typically require longer backward periods to trace back to the CPT.

where the time periods elapsed since air parcels had encountered their LCPs may be months. Such delayed influence is also well-known in the context of the atmospheric 'tape recorder', where water vapor anomalies imprinted at the cold point propagate upward due to the weak tropical upwelling (Mote et al., 1996). Within the ASM anticyclone, weak mixing allows this memory effect to be preserved along upward-moving trajectories, which is also referred to as 'upward spiraling' (Vogel et al., 2019). To further investigate the control of lower stratospheric water vapor mixing ratios by the large-scale temperature field, we now correlate the SAGE III/ISS and MLS water vapor values observed above the tropopause with the respective CPTs either derived from the Lagrangian reconstruction or from the local temperature profiles. Figure 4 presents scatter plots illustrating observed water vapor mixing ratios versus CPTs for the three experiments: Loc, Lag (SAGE III/ISS), and Lag (MLS). Specifically, the grey dots in Fig. 4a-c represent saturation values at local CPTs, while those in

In general, it is known that the Lagrangian temperature history is necessary to explain the dehydration process in the tropical tropopause layer and the observed dryness of the lower stratosphere (Fueglistaler et al., 2005). However, in the Northern hemisphere monsoon circulations the air masses are confined to some degree and it is not clear per se if dehydration and moistening processes are controlled more strongly by local processes (e.g., convection in the monsoons). To investigate this question, Fig. 4 d-i represent the saturation values at Lagrangian CPTs.

Consistent with the results in Fig. 3shows correlations of the SAGE III/ISS and MLS water vapor values observed in UTLS against local cold point temperatures and against LCP temperatures, respectively. Clearly, the correlation between observed water vapor concentrations and local CPTs from LOC cold point temperatures is very weak (Fig. 4a-e)is very weak. The a-c), and the saturation values calculated using local CPTs cold point temperatures (grey points) show large moist biases compared to observed values: 15.14 ppmv on average in the tropics, 6.16 ppmv in the ASM, and 13.48 ppmv in the NAM. In contrast, the reconstructions for LAG show only ~1-2 ppmv dry biases for all regions, significantly reducing the overall biases. Moreover, the correlations between water vapor concentrations and Lagrangian CPTs LCP temperatures are much stronger, ranging from 0.60 for the ASM based on the SAGE III/ISS dataset (Fig. 4e) to 0.78 for the NAM region (Fig. 4f). Notably, the scatter plots for monsoon regions(Fig. 4e, f, h, i) exhibit no significant differences in overall structure compared to those for the tropics (Fig. 4d, g)The reconstructed water vapor biases are also significantly reduces to ~1-2 ppmv (but dryer) on average for all regions.

Hence, we find a similarity between the monsoon regions and the deep tropics regarding the correlation between observed lower stratospheric water vapor mixing ratios and LCP temperatures, but not with local cold point temperatures derived from reanalysis. This suggests that the primary control mechanism for UTLS water vapor in monsoon dehydration in these regions is likely the same as that for the entire tropics governed by non-local processes associated with large-scale transport. However, we note that overshooting convection—often considered a direct injection mechanism for water vapor into the lower stratosphere—is a sub-grid scale process not fully resolved in reanalysis. Therefore, using local cold point temperatures may underestimate the impact of such events, and the weak correlation with local temperatures might not entirely rule out the role of local processes in monsoon regions.

The regression lines for observations versus Lagrangian CPTs-LCP temperatures (blue lines) in Fig. 4d-i-d-i all have smaller slopes than those for the saturation mixing ratios (grey lines), likely due to the influence of points above 19.0 km. The slopes of the regression lines for the Above this altitude, air is more likely to be well-mixed within the stratosphere, making water vapor concentrations less correlated with LCP temperature and more representative of climatological moisture conditions (Fig. S1). The ASM and NAM based on the regression slopes from SAGE III/ISS dataset (Fig. 4e-f) are more aligned with e-f) are closer to the saturation slopes, likely due to less sampling at high altitudes. As altitude increases Moreover, tracing air particles back into the troposphere requires a longer back-trajectory, which introduces more uncertainties in determining CPT. Additionally, air above 19.0 km is more likely to be well-mixed within the stratosphere, which explains why using climatological water vapor concentrations shows better consistency, as depicted in Fig. 2. Thus, instead of being correlated with CPT, water vapor concentrations above 19.0 km appear more related to the climatological moisture conditions within the stratosphere.

Through the discussion above, we assess the performance of the Lagrangian method in water vapor reconstruction from various angles: horizontal and vertical distributions, correlation between reconstructions and observations, and the relationship between altitude, observations and Lagrangian CPT. The overall distributions in both horizontal and vertical directions indicate the satisfactory performance of the Lagrangian CPT reconstruction, effectively capturing the main variations in water vapor concentrations in the boreal summer within monsoon regions. By comparing the results from LAG and LOC, we demonstrate significant advantages of using Lagrangian CPT over local CPT. The use of Lagrangian CPT leads to significantly improved correlations between simulated and observed mixing ratios and substantially reduced biases in determining water vapor concentrations. However, the Lagrangian method also has limitations. Calculating the back-trajectories of each cluster, particularly over a 180-day period for greater accuracy, requires considerable time and storage. More importantly, the results of LAG reveal common dry biases throughout the entire tropics and the UTLS layer. Horizontally, the reconstructions exhibit dry biases of 1-2 ppmv, particularly in the NAM region. Vertically, there are biases of 1-2 ppmv above 16.5 km (around the tropopause) and of 3-5 ppmv below, in the troposphere. Above approximately 19.0 km, climatological water vapor concentrations show greater consistency with observations compared to the reconstructions calculated using Lagrangian CPTs. Without accounting for effects of convection, the Lagrangian method tends to produce dry biased results. The reasonable representation of stratospheric moistening above monsoon regions suggests that using parcels back to the troposphere becomes more uncertain at higher altitudes, as longer back-trajectories driven by reanalysis wind fields and temperature can, to some extent, determine stratospheric water vapor, even during convective seasons and in convective areas.

introduce greater uncertainties in LCP determination.

395

400

405

410

425

#### 420 3.2 Locations of the Lagrangian Cold Pointscold points

The Lagrangian reconstruction not only allows for the reconstruction of reproduces observed water vapor values but also provides insights into the atmospheric traces the regions where dehydration has occurred. Since relevant dehydration seems to have taken occurred before reaching the observation points. Since dehydration events can take place weeks to months before the observation timecarlier, it is valuable to determine the regions of strongest dehydration and whether these regions are strongly localized or more homogeneously crucial to identify the dominant locations of these events and assess whether

they are concentrated in specific regions or more broadly distributed across the tropics. Utilizing all back-trajectories (from experiment LAG), we trace the observations back to the specific locations of their Lagrangian cold points LCPs. Given the large number of such trajectories, we calculate the spatial distribution of these locations using probability density functions (PDFs). The scatter plots of the Lagrangian cold point locations locations of LCPs are shown in Fig. 6a-d-5 (with colors denoting the reconstructed water vapor values), and the corresponding PDFs are presented in Fig. 6e-h.

430

440

The results from the SAGE III/ISS and MLS datasets show similar patterns for both monsoon regions. In the ASM region (Fig. 6a-b), Lagrangian cold points 5c-d), LCPs are spread across the 0-300-30°N zonal band, with most dehydration points situated in the ASM region and some extending into North Africa and North America. According to the PDF of the Lagrangian cold points LCPs in Fig. 6e-f 6c-d, most of the Lagrangian cold points LCPs are located over India and the Bay of Bengal, around 10°-30-30°N, 70°-95-95°E, indicating the primary origin of reconstructed water vapor in the ASM. The For the top 10% of the highest reconstructed water vapor concentrations (exceeding ~6 ppmv), the LCPs are concentrated in the same region (red contour lines), slightly displaced towards higher latitudes. This suggests that the increased water vapor in the ASM, as determined by the reconstruction method, is primarily attributed to dehydration processes occurring in the vicinity of the monsoon over Asia. South Asia. According to Konopka et al. (2023), the 'dehydration carousel' mechanism within the ASM anticyclone plays a key role in shaping the distribution of water vapor entering the stratosphere, that is, while deep convection supplies moisture to the upper troposphere, the coldest regions near the monsoon's southern vicinity act as primary dehydration sites. Air parcels that undergo dehydration in these regions can later be transported within the anticyclone and ascend into the stratosphere, contributing to the observed high water vapor concentrations in the lower stratosphere.

The backward time length required for air parcels observed at 16.5km to reach these Lagrangian cold points LCPs is shown in Fig. S2a-b S2a-b, indicating that the dehydration processes occur over a timescale of days to weeks before the air parcels reach the observation points. Other Lagrangian cold points LCPs, located further away and with lower reconstructed water vapor concentrations (1-5-1-5 ppmv), correspond to longer time periods (1-6-1-6 months) between the dehydration event and observation. While these air parcels with low water vapor air parcels are not the primary factor for the monsoon moist anomalies, their contribution to the final reconstructions water vapor budget highlights the need to extend the simulated backward time period, especially considering the improvements in correlation coefficients shown in Fig. 3-3. These findings reinforce the idea that the ASM anticyclone serves as a crucial transport pathway for air into the stratosphere, while dehydration near its vicinity regulates the amount of water vapor that ultimately enters the stratospheric circulation.

For the NAM region (Fig. 6e-d), significant scatter is 5e-f), a significant number of LCPs are observed across North America, with overall patterns extending throughout the 0-30. Remarkably, the region of occurrence of LCPs extends throughout the 0-30°N zonal band, including into South Asia. Surprisingly, the even into southern Asia. The PDFs in Fig. 6g-h e-f indicate that the primary dehydration center is in the ASM region, meaning that most air parcels in the NAM UTLS experienced dehydration in South southern Asia. Focusing on the top 10% highest reconstructed water vapor concentrations (Fig. 6g-he-f), we identify two leading centers for the Lagrangian cold pointsLCPs. One center remains in South is located in southern Asia, a similar region to the ASM dehydration center but displaced slightly southeastward. The other, more significant center is near the NAM itself, which is likely the main contributor to the increase in reconstructed water vapor concentrations in the NAM.

This suggests that the increase in reconstructed water vapor concentrations in the NAM region is primarily influenced by local tropopause temperatures, with additional moisture contributions from transport from South southern Asia. In the trajectory simulations, the average backward period required to trace observed air parcels back to their Lagrangian cold points LCPs for the NAM is ~45 days (Fig. S2e-dc\_d). This indicates that the temperatures used to reconstruct the water vapor at those Lagrangian cold points LCPs are partially from June or even earlier, which are lower than the temperatures in August, leading to lower reconstructions.

In summary, the analysis of Lagrangian cold points along back-trajectories reveals significant insights into the distribution of the cold temperature regions and corresponding dry points that contribute to UTLS water vapor within The locations of LCPs for the tropics (Fig. 5a-b) resemble an ensemble of those found in the ASM and NAM, suggesting that dehydration predominantly occurs near the monsoon regions. Specifically, regions over India and the Bay of Bengal are crucial for the water vapor budget in the ASM. For the NAM region, both local sources in the Western Pacific and Gulf of Mexico, as well as sources over South Asia, determine the final water vapor values. The combination of long-range transport from remote regions and local convection—particularly, with remote influences being more substantial for the NAM than the ASM—appears to be decisive for the final moisture composition within the anticyclones. A remaining question is how the Lagrangian reconstruction resolves the contribution of local convection, which will be discussed in the next section. Additionally, the PDFs for the tropics (Fig. 6a-b) show that LCPs are highly concentrated in southern Asia, even when considering only the top 10%, reinforcing the significance of southern Asia as a major dehydration center of the monsoon regions.

## 4 Discussion: Lagrangian reconstruction and convection

## 3.1 Lagrangian reconstruction and convection

465

475

480 To We further investigate the cause of the common dry biases and the related effects of convection relation between the dry bias in the reconstructions and convection as a potential moistening process. Therefore, we follow recent studies (e.g., Randel et al., 2015; Peña-C (e.g., Randel et al., 2015; Peña-Ortiz et al., 2024) and use OLR as a proxy for convection . We specifically analyze the potential influence of convection on the Lagrangian water vapor reconstruction, intensity, with high OLR values corresponding to weak convection and low OLR values corresponding to strong convection. Note that while OLR is a commonly used proxy, it has limitations—it primarily captures cold cloud tops and may miss warm-topped or thin convection, leading to potential biases 485 in certain regions or conditions (e.g., Liu et al., 2007). Randel et al. (2015) used MLS observations from May to September (2005-2013) to obtain time series of UTLS (100 hPa) water vapor concentrations above in the ASM, separating specific wet and dry phases to reveal the corresponding anomalous OLR-convection patterns. Their findings indicate that OLR anomalies exhibit a convection exhibits a west-east dipole structure over the whole ASM region. The decrease in OLR anomalies (indicating strong convection) strong convection over the eastern part of the dipole (20-30°N, 490 80-11080-110°E) corresponds to the dry phase a dry phase in the ASM UTLS (i.e. low UTLS water vapor mixing ratios over the whole ASM) and vice versa. We conduct a similar analysis to derive OLR indices and then composite water vapor concentrations within the entire ASM region (15–35°N, 60–140°E) for observations from SAGE III/ISS and the reconstructions. Two OLR indices are defined according to the dipole structure—: an OLR-West and index quantifies convection intensity in the western part, while an OLR-East index quantifies convection intensity in the eastern part of the ASM (Sect. 2.2)—and

. These indices are used to select days with high-OLR (relatively weak convection (OLR ≥ 1.5 standard deviations) and low-OLR (strong convection (OLR ≤ -1.5 standard deviations). The west-east shifts in convection, as reflected in these OLR indices, may be related to different modes of the ASM anticyclone (Honomichl and Pan, 2020).

Figure 7 shows presents water vapor observations and reconstructions averaged over the 0–10 days following high and low OLR events. Note that anomalously low OLR corresponds to increased convection, and vice-versa0–10 days following strong and weak convection events. Consistent with Randel et al. (2015), using the OLR-East index shows The composites for convection intensity in the eastern part of the ASM reveal that observed water vapor mixing ratios are drier for strong-convection days than those composited for weak-convection days below 16.5 km (-100 hPa), composited for low-OLR days (strong convection), are dryer than those for high-OLR days, with the highest difference of 6.6 ppmv at 15.5-17.5 km (Fig. 7a). This drying effect of convection is weak within the stratosphere at 17.5 km (-0.21 ppmv) but increases to -6.6 ppmv at 15.5 km within troposphere. The profiles using the OLR-West index Conversely, the composites for convection intensity in the western part of the ASM show the opposite results, with increased moisture for low OLR corresponding to strong convection trend: composited water vapor concentrations for strong-convection periods are higher than those for weak-convection periods below 17.5 km (Fig. 7b). Our results confirm are consistent with Randel et al. (2015), demonstrating that strong convection in the eastern part of the ASM is associated with drying of the UTLS, while the strong convection shifting to the western part a dry UTLS, whereas a westward shift of strong convection is associated with moistening of the a moist UTLS.

The right panels of Fig. 7 show the results for display the reconstructed water vapor profiles. Using either the OLR-East or OLR-West index does not significantly affect the reconstructions or the differences between strong and weak convection periods. This suggests that neither Below the lapse rate tropopause (yellow dashed lines), the reconstructions show an insignificant response to changes in convection intensity compared to the observations. This finding suggests that the reconstruction is not capable of catching the influence of the west-east shift nor the intensity of convection has a substantial impact on the reconstructions of convection in the ASM region. This finding indicates that These differences between the reconstruction and observations concerning the effect of convection in the ASM region highlight a key limitation of the simple Lagrangian water vapor reconstruction methodfails to capture the: while it effectively represents large-scale dehydration and transport processes, it struggles to accurately represent convective moistening and dryingprocesses associated with convection and ice injection in the monsoon regions, along with localized processes in the upper troposphere. This limitation may be due to ERA5's inadequate representation of temperature variations associated with convection variability or with the missing representation of ice injection and microphysics in the simplified dehydration method, is also evident in Fig. 2b, where the reconstructions exhibit increasing dry biases from less than 2 ppmy in the stratosphere (above 17.5 km) to a maximum of 5 ppmy in the troposphere (15.5 km). This limitation could also be a primary cause of the common dry biases in Lagrangian reconstructions and the limited coverage of reconstructed water vapor anomalies over the ASM, as compared with observations in Fig.

Figure 8 further examines the relation between convection intensity (based on the OLR-indices defined above) and the biases in reconstructed water vapor concentrations at 16.5 km based on SAGE III/ISS. <u>le and g</u>Overall, convection in the eastern

part of the ASM is stronger (OLR 200–230 W/m²) than in the western part of the ASM (OLR 240–280 W/m²). However, no significant correlation of the reconstruction bias to convection in the eastern monsoon region is found (Fig. 8a), suggesting that eastern convection does not significantly impact the reconstruction performance. In contrast, convection in the western monsoon region exhibits a significant correlation with the reconstruction bias, with a correlation coefficient of 0.73 (Fig. 8b). Despite being weaker than eastern convection, western convection has a stronger influence on the biases, leading to increased dry biases in the reconstructions following periods of strong convection. This pattern is also evident when comparing Fig. 7b and 7d. In addition, the correlation between reconstructed biases and convection intensity in the western monsoon region (OLR-West index) varies with altitude, with correlation coefficients of 0.47, 0.73\* (with a star indicating statistical significance at the 95% confidence level based on the Student's t-test), 0.46, and 0.24 from 16.0 km to 17.5 km (with 0.5 km interval). With the exception of 16.5 km, the correlations at other levels do not pass the significance test. The correlation maximum at 16.5 km highlights the relevance of convection-driven processes near the tropopause. We attribute this altitude-dependent behavior to different atmospheric regimes: at and below 16.5 km, convection has a stronger influence, whereas above 17.0 km, the Lagrangian reconstruction becomes less sensitive to convection and is dominated by large-scale transport and the trajectory history of air parcels.

Additionally, the water vapor reconstructions for the NAM region are less satisfactory compared to the ASM.In the NAM region, the anomalies are only partially reproduced, while the ASM anomalies are nearly fully captured (

## 545 4 Discussion

530

535

540

550

555

560

As shown in Fig. 1 e-d, g-h). Our results show that the correlation coefficients between the Lagrangian CPTs and observed water vapor concentrations are highest for the NAM region (Fig. and Fig. 4f and i)2, the reconstructions exhibit a consistent dry bias (~1.5 ppmv) above the cold point tropopause in both the ASM region and throughout the broader tropics. A similar dry bias has been reported by Liu et al. (2010), who suggested that incorporating cloud microphysical processes could significantly reduce this bias by relaxing the assumption of instantaneous dehydration to the saturation mixing ratio. Similarly, Schoeberl et al. (2013) implemented a Lagrangian cloud model that simulates the conversion of excess water vapor to ice, and setting parcels to saturation within convection zones. They showed that including such simplified Lagrangian cloud model improves agreement with MLS observations. Also other studies have shown that a simple allowance for supersaturation at LCPs can substantially reduce the dry bias (Schiller et al., 2009; Ploeger et al., 2011). However, despite this strong correlation, the reconstructions based on the Lagrangian CPTs perform less satisfactorily. This discrepancy, along with the biases observed while effective, this approach remains a simplified representation of the complex microphysical processes that influence dehydration efficiency, as well as of other small-scale processes like turbulence and mixing (Poshyvailo et al., 2018). Such underrepresented processes can contribute to the dry bias in our reconstructions.

While the simplified Lagrangian method performs well in reconstructing the moist anomaly in the ASM, it struggles with representing the moisture budget in the NAMregion, could be linked to several factors: errors in representing local temperature variability and convection, or inaccuracies in transport processes. Homeyer et al. (2024) suggest that the processes driving

stratospheric hydration during NAM convection often involve ice sublimation without significant changes in other trace gases, indicating a unique characteristic of NAM events that may not be captured adequately in standard reconstructions. suggesting that different mechanisms may be at play in this region. Previous studies indicate that, in boreal summer, the ASM is characterized by a strong anticyclonic circulation at 100 hPa, along with a smaller, approximately symmetric anticyclone in the Southern Hemisphere subtropics, which can be explained by the dynamical structure of the Gill response (Park et al., 2007). In contrast, the geopotential height over North America at 100 hPa exhibits no such structure, highlighting a fundamental difference between the NAM and ASM from a large-scale circulation perspective. Also, studies by Smith et al. (2017) and O'Neill et al. (2021) show that frequent deep convection over North America and particularly intense convective events, can transport water vapor into the lower stratosphere. These findings suggest that deep, potentially overshooting convection might play a more crucial role in the UTLS water vapor budget in the NAM compared to other regions and may be the primary driver of the large biases observed in Lagrangian reconstructions.

Additionally, as suggested by our trajectory simulation results, the long-range transport from South southern Asia to the NAM region appears to significantly influence NAM water vapor concentrations, meaning that. On the one hand, the significant fraction of air masses experiencing dehydration over southern Asia before reaching North America implicates the dominant role of the Asian monsoon in controlling the moisture entering the stratosphere during boreal summer, which is consistent with previous studies (Fueglistaler et al., 2004; Ploeger et al., 2013). On the other hand, the limited performance of the reconstruction for the NAM may be attributed to errors in ERA5 wind and transport processes could also contribute to these biases. Homeyer's findings emphasize the role winds, which can introduce biases in transport modeling, and diabatic heating rates. Additionally, the presence of multiple, competing mechanisms within convection events, which may complicate the may further complicate the accurate representation of long-range transport effects in models. Further investigation of other in models (Homeyer et al., 2024).

Moreover, previous studies have shown that trajectories computed with 6-hourly reanalysis data exhibit transport errors and warm biases of cold point tropopause compared to those calculated with higher temporal resolution (1-hourly) data (Pisso et al., 2010; Bourguet and Linz, 2022). These biases could lead to inaccuracies in simulating dehydration processes and ultimately impact the reconstructed water vapor distribution. Investigating additional tracers originating from Asia could help to clarify whether the assess whether long-range transport from Asia to the NAM region and its remote influence on NAM water vapor levels is accurately represented.

are accurately captured in current trajectory-based reconstructions.

#### 590 5 Conclusions

565

570

575

580

585

This study investigates the performance of Lagrangian reconstructions of UTLS water vapor in the boreal summer monsoons over Asia and North America. The reconstructed water vapor fields are evaluated using SAGE III/ISS and MLS observations, with SAGE III/ISS providing higher vertical resolution and revealing finer-scale structures in the UTLS. Our results demonstrate

the effectiveness of the Lagrangian method in capturing tropical UTLS water vapor variations and structures, with improved performance from the tropopause upwards.

Overall, the Lagrangian approach, including the temperature history of air masses, is found to be equally effective in reconstructing water vapor mixing ratios in the Asian monsoon as in the deep tropics. Given that most air parcels undergo dehydration in the southern vicinity of the ASM, we conclude that UTLS water vapor concentrations in the ASM are largely governed by large-scale transport through the cold tropopause in this region. A systematic dry bias in reconstructions in the ASM of approximately 1.5 ppmv is similar to dry biases found previously for lower stratospheric water vapor in the deep tropics. Nevertheless, the Lagrangian reconstruction reproduces the anomalies of stratospheric water vapor mixing ratios in the ASM well and captures more than two-thirds of the observed moist anomalies. Reconstructions using larger trajectory ensembles for each satellite observation point show significantly better performance compared to reconstructions based on smaller ensembles.

Conversely, the Lagrangian method fails to reproduce the observed moistening in the NAM region. The ERA5-driven trajectory simulations suggest that while the highest UTLS water vapor concentrations in the NAM are primarily controlled by local tropopause temperatures over America, most air masses in the NAM region are remotely influenced by long-range transport from southern Asia and the associated tropopause temperatures there. We hypothesize that the failure of the water vapor reconstruction in the NAM UTLS is likely due to an underestimation of local moistening processes such as deep convection and ice injection, which are not explicitly included in the reconstruction method. Additionally, errors in the cross-Pacific long-range transport could be another factor affecting the particularly large dry bias in the NAM reconstructions.

Finally, based on analyses of convective variability, using outgoing longwave radiation as an indicator of convection, we assessed the impact of convection on UTLS water vapor variability and on the bias in the Lagrangian reconstructions. Based on observations from SAGE III/ISS we can confirm the findings of Randel et al. (2015) which show that strong convection in the eastern part of the ASM leads to UTLS drying, whereas a westward shift of convection results in UTLS moistening. Correlation analyses reveal that the biases in Lagrangian reconstructions are significantly linked to the intensity of convection in the western region of the ASM, with stronger convection associated with increased dry biases. In contrast, no clear influence on the reconstruction bias is found for convection in the eastern part of the ASM. Hence, it is likely the underestimated moistening effect of ice injection of convection in the western region of the Asian monsoon which controls the dry bias of Lagrangian reconstructions in the ASM. Investigating similar connections between model dry biases and convective intensity in other regions appears promising for improving simulations of the UTLS moisture budget.

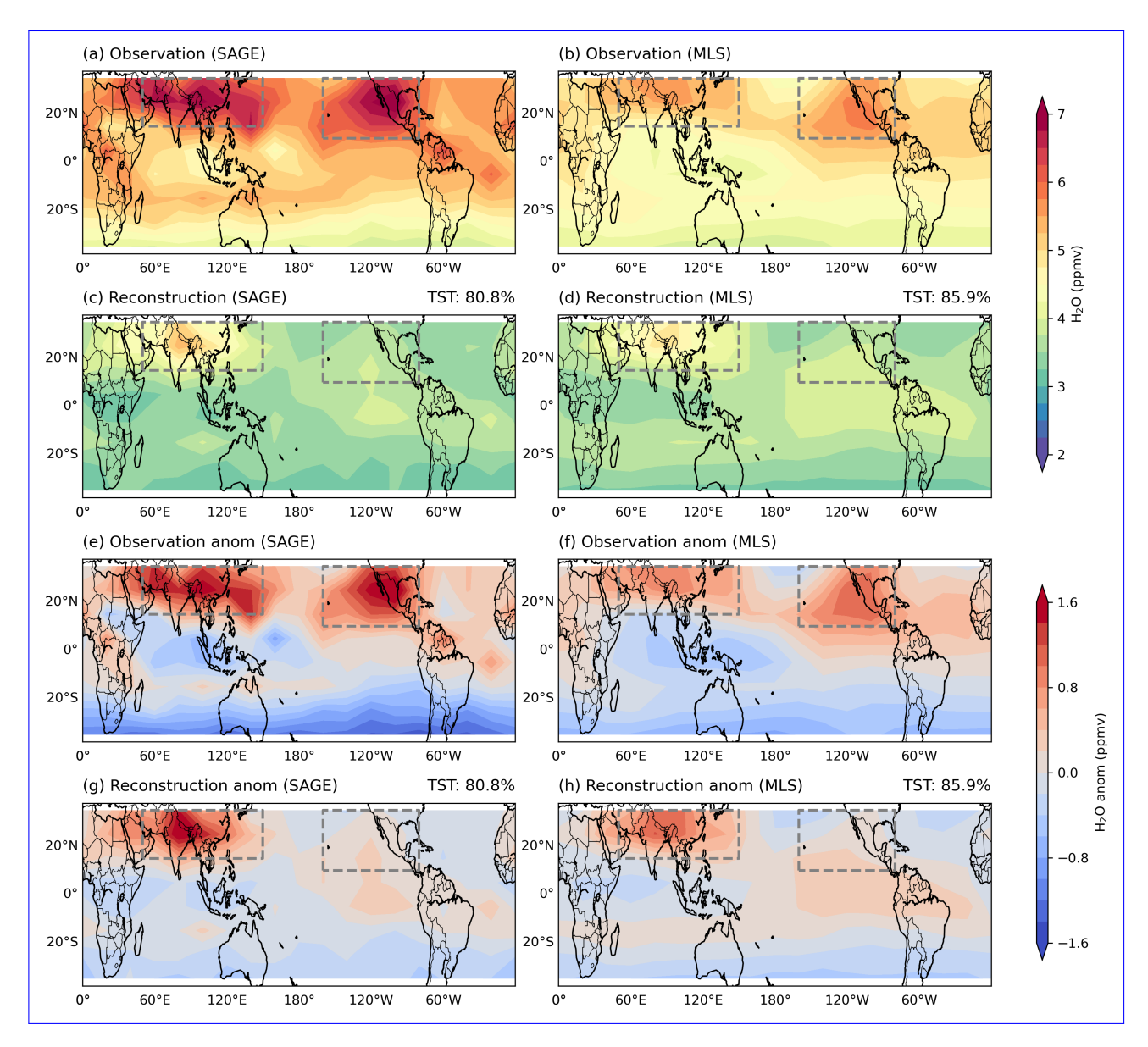


Figure 1. Horizontal distribution of water vapor concentrations and anomalies in August. Observed water vapor (H<sub>2</sub>O) concentrations (a-ba-b), the reconstructed concentrations of Experiment LAG (e-dc-d) and corresponding anomalies (e-he-h) based on SAGE III/ISS at 16.5 km (left) and MLS at ~ 16.3 km (right). The anomalies are calculated by subtracting the average values of the entire tropics (35°S to 35°N). Grey boxes in each subplot show the defined area of ASM (15°-35-35°N, 50°-150-150°E) and NAM (10°-35-35°N, 160°-80-80°W). Reconstructions in this figure use both TSTs and non-TSTs, the portions of TST are shown with upper right strings of e-d-c-d and g-hg-h.

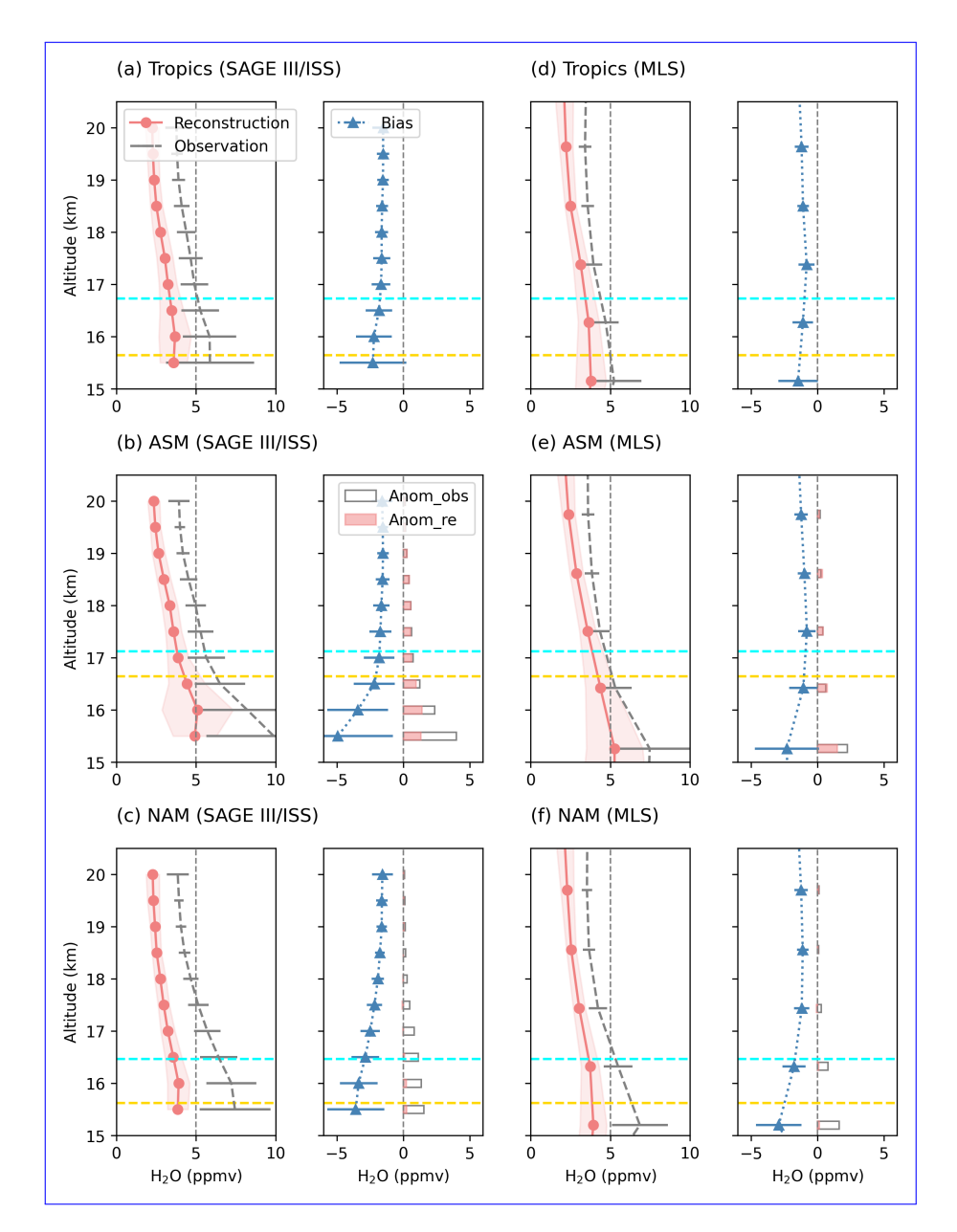
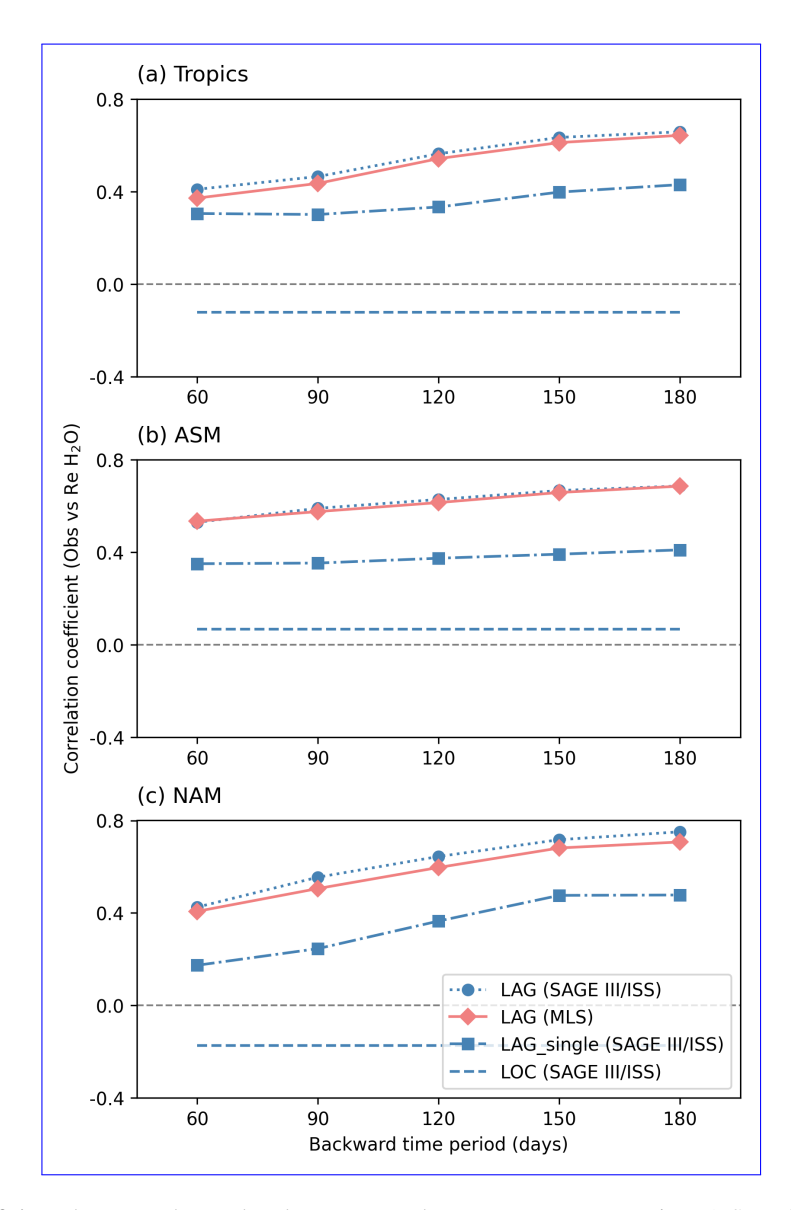


Figure 2. Vertical profiles of water vapor (H<sub>2</sub>Q) concentrations in August. For each subplot, it shows observed water vapor concentrations (grey dotted lines), reconstructed concentrations of Experiment LAG (red coral lines, including both TSTs and non-TSTsTST-only), and the bias between them (reconstructed values substract subtract observed values, blue lines). Upper, middle and lower columns show the averaged values in the tropics (35°S-35S-35°N), ASM and NAM, from SAGE III/ISS (left panels) and MLS (right panels). The cyan horizontal dashed lines indicate the position of the climatological cold point tropopause in August, while the yellow horizontal dashed lines represent the lapse rate tropopause defined by WMO. Both tropopauses are derived from ERA5 reanalysis. For the ASM (b, e) and NAM (c, f), the gray bars in the right sub-panels represent the observed anomalies, while the coral bars indicate the reconstructed anomalies. The anomalies are calculated by subtracting the corresponding mean values in the tropics, as shown in (a) and (d).



**Figure 3.** Correlation coefficients between observed and reconstructed water vapor concentrations (TST-only). Upper, middle and lower panels show the correlation coefficients between 15.5-20.0 km within in entire tropics (a), ASM (b) and NAM (c), respectively. Red diamonds represent the results of Experiment LAG based on MLS dataset. Blue crosses, squares and rounds represent the results based on SAGE III/ISS dataset of LOC, LAG\_single and LAG, respectively. The LOC values remain constant as they do not vary with backward time in Lagrangian experiments.

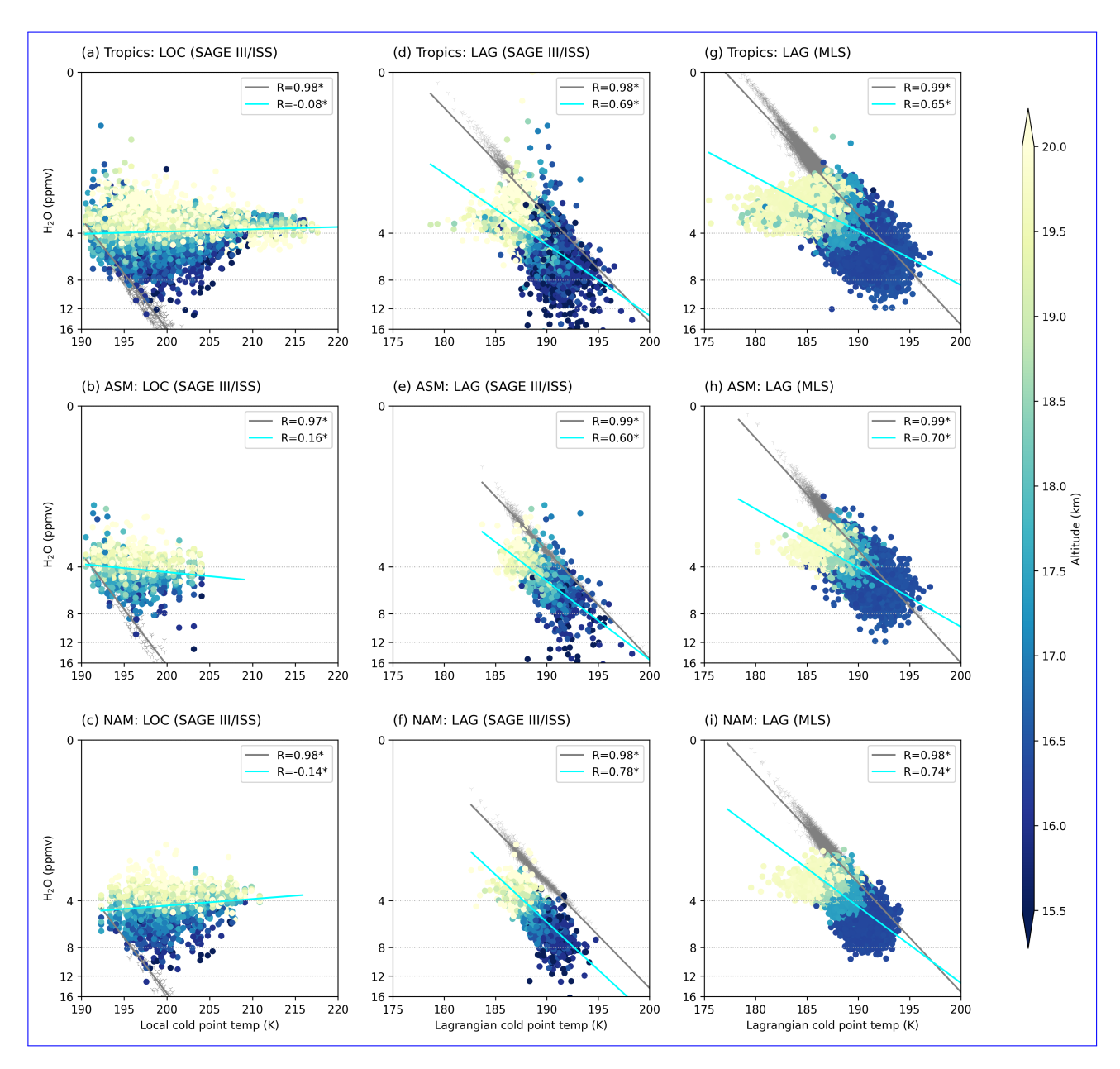


Figure 4. Scatters of water vapor (H<sub>2</sub>O) concentrations (TST-only) vs dry cold point temperatures. Left: water vapor concentrations from SAGE III/ISS vs local dry cold point temperatures (Experiment LocLOC). Middle: water vapor concentrations from SAGE III/ISS vs Lagrangian dry cold point temperatures (Experiment LAG based on SAGE III/ISS). Right: water vapor concentrations from MLS vs Lagrangian dry cold point temperatures (Experiment LAG based on MLS). Coloured points indicate the observed water vapor concentrations with the colour showing altitudes of the points. Grey dots represent reconstructed concentrations (saturation). The legends show the correlation coefficients and stars indicate statistical significance at the 95% confidence level based on the Student's t-test.

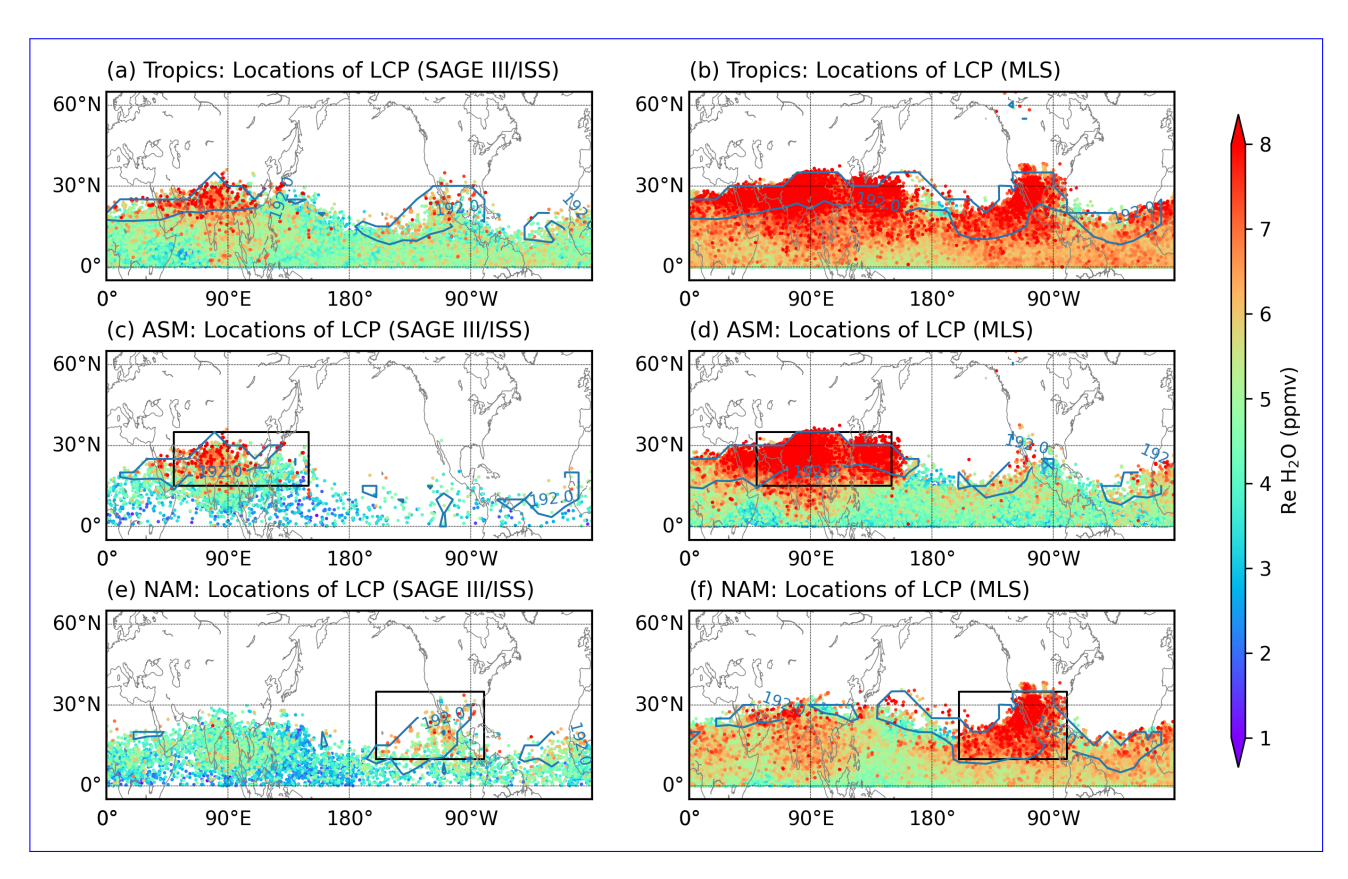


Figure 5. Horizontal distributions of the locations of the Lagrangian cold points (LCPs) used for water vapor (H2O) reconstruction at 16.5 km, derived from Experiment Lag and their probability density functions (PDFs)LAG. The locations of the LCPs are shown with colors representing the reconstructed water vapor concentrations, with starting points in ASM the entire tropics (a, b)and NAM. (a, d) and NAM. (e, f). The scatters are plotted in ascending sequence according to the values of reconstructions. The blue contour lines in a d-represent the CPTs at a cold point temperatures of 192 K. The PDFs of these locations are presented for ASM (e, f) and NAM (g, h), and the red contour lines in these plots represent the PDFs of the locations with the top 10% highest reconstructed water vapor concentrations. The left panels (a, c, e, g) show results based on SAGE III/ISS, while the right panels (b, d, f, h) show results based on MLS data. The black boxes indicate the original regions of starting points.

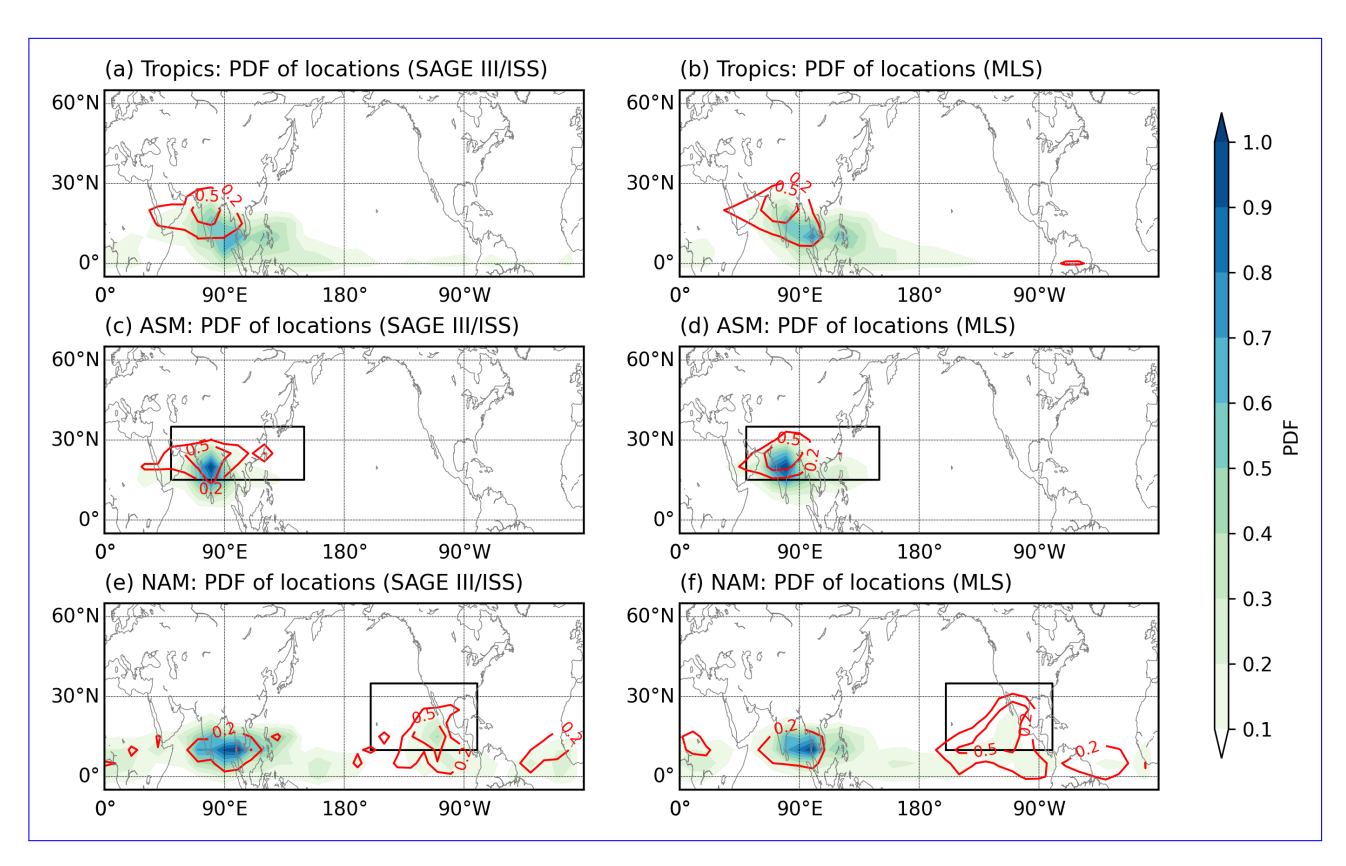


Figure 6. Vertical profiles Probability density functions (PDFs) of water vapor concentrations under the influence-locations of convention within the ASM region, based on SAGE III/ISS datasetLagrangian cold points (LCPs) in Fig. 5. The left panels show observed water vapor profiles averaged during high-OLR days PDFs are presented for the entire tropics (weak convention)a, low-OLR days (strong convectionb), and the difference, with OLR indices averaged within the eastern part ASM (ac, d) and western part NAM (b). Right panels show reconstructed water vapor profiles averaged during high-OLR dayse, low-OLR daysf), and with red contour lines representing the difference, PDFs of the locations with OLR indices averaged within the eastern part top 10% highest reconstructed water vapor concentrations. The left panels (a, c, e) and western part show results based on SAGE III/ISS, while the right panels (b, d, f) show results based on MLS data.

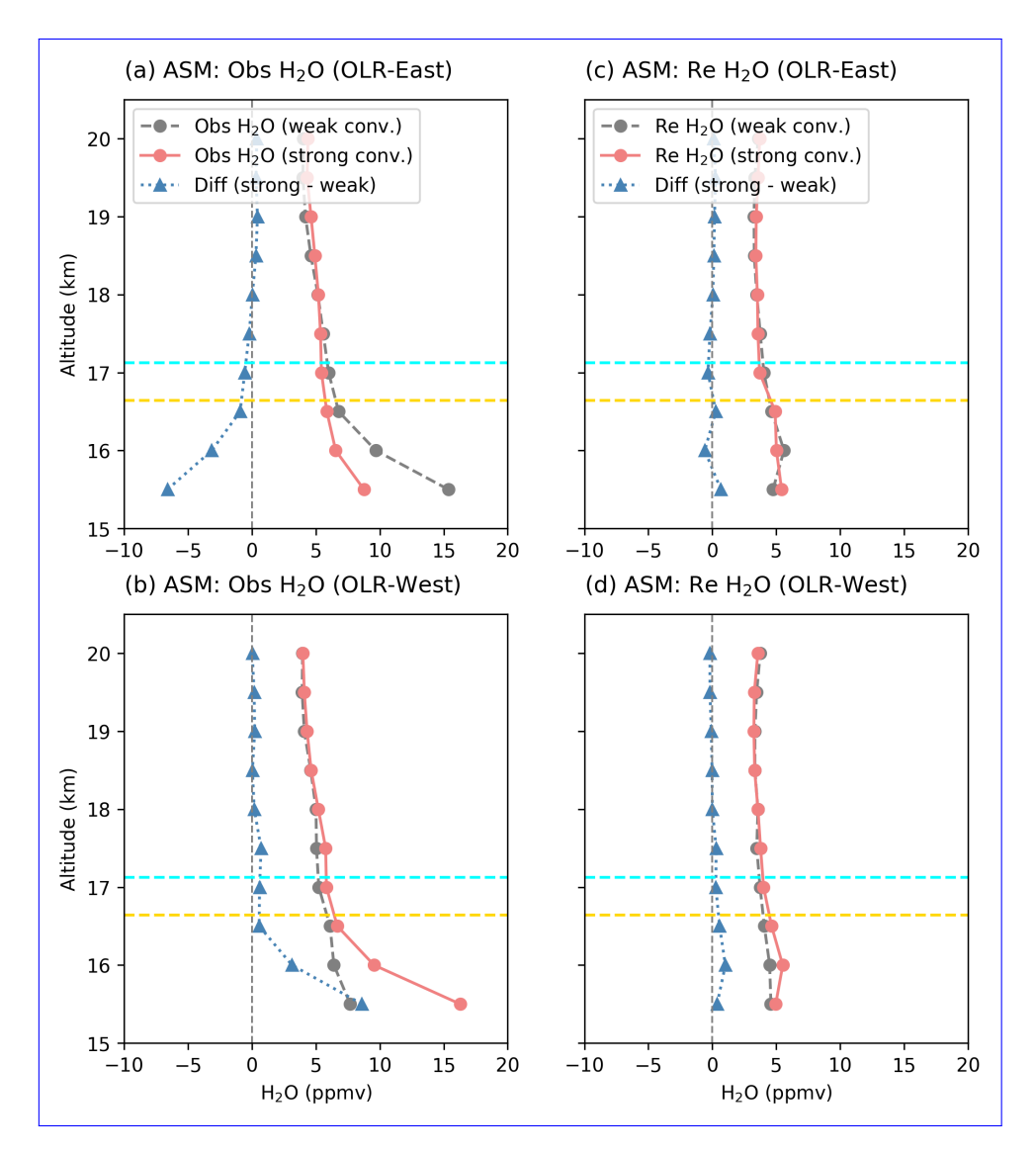
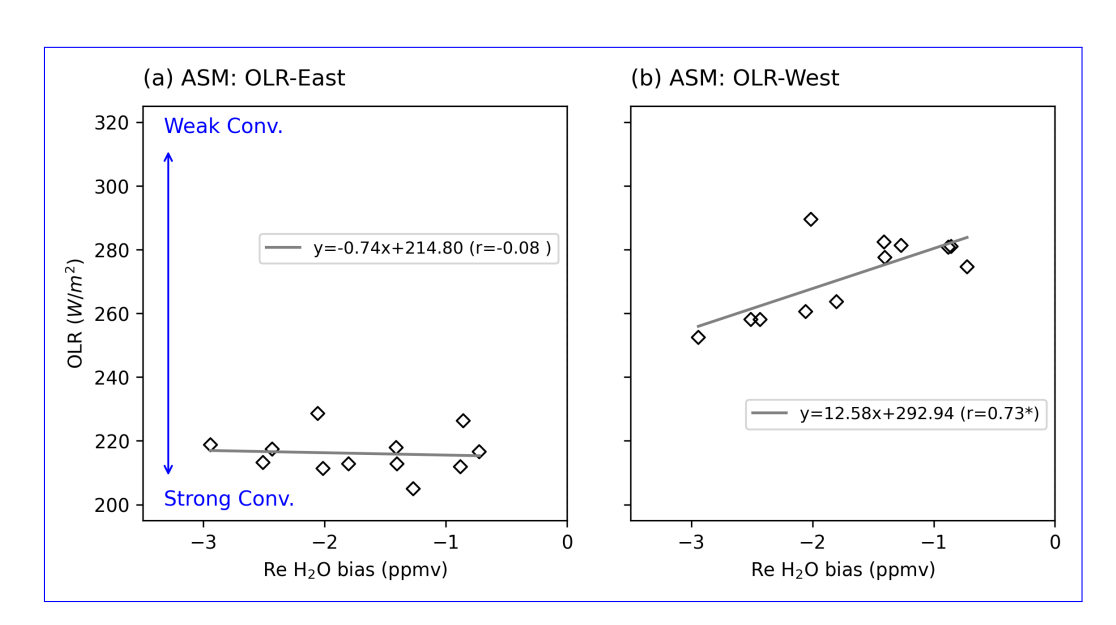


Figure 7. Vertical profiles of water vapor (H<sub>2</sub>O) concentrations under the influence of convection within the ASM region, based on SAGE III/ISS dataset. The left panels show observed water vapor profiles averaged during weak-convection (high-OLR) and strong-convection (low-OLR) days, along with their differences, for OLR-West (a) and OLR-East (b) indices, where OLR is averaged over the western and eastern regions, respectively. Right panels show reconstructed water vapor profiles averaged during weak-convection days, strong-convection days, and their differences, for OLR-West (c) and OLR-East (d) indices. Same as in Fig. 2, the cyan and yellow horizontal dashed lines indicate the positions of the climatological cold point tropopause and lapse rate tropopause in August, respectively.



**Figure 8.** Scatter plots of OLR (convection intensity) versus biases in reconstructed water vapor concentrations (SAGE III/ISS) at 16.5 km for the ASM. Panels (a) and (b) correspond to results using OLR-East and OLR-West, respectively. The biases are half-monthly averaged, while OLR values are first averaged over the 0–10 days preceding each date and then half-monthly averaged. The legends display the regression line equations and correlation coefficients, with a star indicating statistical significance at the 95% confidence level based on the Student's t-test.

Code and data availability. The CLaMS model is available in the CLaMS git database. Detailed information is available at https://clams.icg.kfa-juelich.de/CLaMS/GitLabInstructions. ERA5 reanalysis data are available from the European Centre for Medium-range Weather Forecasts (https://apps.ecmwf.int/data-catalogues/era5/?class=ea), last access: 03 August 2024). The MLS v5.0 water vapor data used in this study are available from NASA's Earthdata website (https://www.earthdata.nasa.gov/learn/find-data/near-real-time/mls). SAGE III/ISS Level 2 Solar Event Species Profiles (HDF5) Version 5.3 data can be accessed through NASA's Atmospheric Science Data Center (https://asdc.larc.nasa.gov/project/SAGE%20III-ISS/g3bssp\_53). The NOAA CPC OLR data are available at (https://psl.noaa.gov/data/gridded/data.cpc\_blended\_olr-2.5deg.html).

Author contributions. H. W. carried out the analysis and wrote the original draft of the manuscript. P. K. and F. P. supervised the research,
 630 contributing ideas, guidance, and discussions throughout the study, and assisted with iterative revisions. M. P., M. T., C. P., and N. P. provided comments and suggestions during the manuscript revision. All authors contributed to discussions and final revisions of the paper.

Competing interests. The authors declare no competing interests.

625

Acknowledgements. The authors would like to express their gratitude to the European Centre for Medium-Range Weather Forecasts (ECMWF) for providing meteorological analysis for this study. We extend our appreciation to Nicole Thomas for her exceptional programming support.

Additionally, we thank ChatGPT (https://chat.openai.com, last accessed: 2 October 2024 March 2025) for their assistance in refining the final text. The CPC Daily Blended Outgoing Longwave Radiation (OLR) - 2.5 degree data was kindly provided by the NOAA PSL, Boulder, Colorado, USA, via their website at https://psl.noaa.gov. FP acknowledges support by the Deutsche Forschungsgemeinschaft (TPChange grant, The Tropopause Region in a Changing Atmosphere, DFG TRR 301, Project-ID 428312742).

#### References

670

- Avery, M., Davis, S., Rosenlof, K., Ye, H., and Dessler, A.: Large anomalies in lower stratospheric water vapour and ice during the 2015-2016 El Ninō, Nature Geoscience, 10, 405–409, https://doi.org/10.1038/ngeo2961, cited By 67, 2017.
  - Bannister, R., O'Neill, A., Gregory, A., and Nissen, K.: The role of the south-east Asian monsoon and other seasonal features in creating the 'tape-recorder' signal in the Unified Model, Quarterly Journal of the Royal Meteorological Society, 130, 1531 1554, https://doi.org/10.1256/qj.03.106, cited by: 63, 2004.
- Bourguet, S. and Linz, M.: The impact of improved spatial and temporal resolution of reanalysis data on Lagrangian studies of the tropical tropopause layer, Atmospheric Chemistry and Physics, 22, 13 325–13 339, https://doi.org/10.5194/acp-22-13325-2022, cited By 6, 2022.
  - Brewer, A.: Evidence for a world circulation provided by the measurements of helium and water vapour distribution in the stratosphere, Quarterly Journal of the Royal Meteorological Society, 75, 351–363, https://doi.org/10.1002/qj.49707532603, cited By 831, 1949.
- Cisewski, M., Zawodny, J., Gasbarre, J., Eckman, R., Topiwala, N., Rodriguez-Alvarez, O., Cheek, D., and Hall, S.: The stratospheric aerosol
   and gas experiment (SAGE III) on the International Space Station (ISS) Mission, in: Sensors, Systems, and Next-Generation Satellites
   XVIII, vol. 9241, pp. 59–65, SPIE, 2014.
  - Clemens, J., Ploeger, F., Konopka, P., Portmann, R., Sprenger, M., and Wernli, H.: Characterization of transport from the Asian summer monsoon anticyclone into the UTLS via shedding of low potential vorticity cutoffs, Atmospheric Chemistry and Physics, 22, 3841 3860, https://doi.org/10.5194/acp-22-3841-2022, cited by: 3; All Open Access, Gold Open Access, Green Open Access, 2022.
- Davis, S., Damadeo, R., Flittner, D., Rosenlof, K., Park, M., Randel, W., Hall, E., Huber, D., Hurst, D., Jordan, A., Kizer, S., Millan, L., Selkirk, H., Taha, G., Walker, K., and Vömel, H.: Validation of SAGE III/ISS Solar Water Vapor Data With Correlative Satellite and Balloon-Borne Measurements, Journal of Geophysical Research: Atmospheres, 126, https://doi.org/10.1029/2020JD033803, cited by: 11; All Open Access, Bronze Open Access, 2021.
- Fu, R., Hu, Y., Wright, J. S., Jiang, J. H., Dickinson, R. E., Chen, M., Filipiak, M., Read, W. G., Waters, J. W., and Wu, D. L.: Short circuit of water vapor and polluted air to the global stratosphere by convective transport over the Tibetan Plateau, Proceedings of the National Academy of Sciences of the United States of America, 103, 5664 5669, https://doi.org/10.1073/pnas.0601584103, cited by: 268; All Open Access, Green Open Access, 2006.
  - Fueglistaler, S. and Haynes, P.: Control of interannual and longer-term variability of stratospheric water vapor, Journal of Geophysical Research Atmospheres, 110, 1 14, https://doi.org/10.1029/2005JD006019, cited by: 161; All Open Access, Bronze Open Access, 2005.
- Fueglistaler, S., Wernli, H., and Peter, T.: Tropical troposphere-to-stratosphere transport inferred from trajectory calculations, Journal of Geophysical Research: Atmospheres, 109, D03 108 1–16, https://doi.org/10.1029/2003jd004069, cited by: 162; All Open Access, Bronze Open Access, 2004.
  - Fueglistaler, S., Bonazzola, M., Haynes, P. H., and Peter, T.: Stratospheric Water Vapor Predicted From the Lagrangian Temperature History of Air Entering the Stratosphere in the Tropics, Journal of Geophysical Research Atmospheres, https://doi.org/10.1029/2004jd005516, 2005.
  - Fueglistaler, S., Dessler, A., Dunkerton, T., Folkins, I., Fu, Q., and Mote, P.: Tropical tropopause layer, Reviews of Geophysics, 47, https://doi.org/10.1029/2008RG000267, cited by: 743; All Open Access, Bronze Open Access, 2009.
  - Hasebe, F. and Noguchi, T.: A Lagrangian description on the troposphere-to-stratosphere transport changes associated with the stratospheric water drop around the year 2000, Atmospheric Chemistry and Physics, 16, 4235 4249, https://doi.org/10.5194/acp-16-4235-2016, cited by: 5; All Open Access, Gold Open Access, Green Open Access, 2016.

- Haynes, P. and Anglade, J.: The vertical-scale cascade in atmospheric tracers due to large-scale differential advection, Journal of the Atmospheric Sciences, 54, 1121 1136, https://doi.org/10.1175/1520-0469(1997)054<1121:TVSCIA>2.0.CO;2, cited by: 125; All Open Access, Bronze Open Access, 1997.
- Hersbach, H., Bell, B., Berrisford, P., Hirahara, S., Horányi, A., Muñoz-Sabater, J., Nicolas, J., Peubey, C., Radu, R., Schepers, D., Simmons, A., Soci, C., Abdalla, S., Abellan, X., Balsamo, G., Bechtold, P., Biavati, G., Bidlot, J., Bonavita, M., De Chiara, G., Dahlgren, P., Dee, D., Diamantakis, M., Dragani, R., Flemming, J., Forbes, R., Fuentes, M., Geer, A., Haimberger, L., Healy, S., Hogan, R. J., Hólm, E., Janisková, M., Keeley, S., Laloyaux, P., Lopez, P., Lupu, C., Radnoti, G., de Rosnay, P., Rozum, I., Vamborg, F., Villaume, S., and Thépaut, J.-N.: The ERA5 global reanalysis, Quarterly Journal of the Royal Meteorological Society, 146, 1999 2049, https://doi.org/10.1002/qj.3803, cited by: 11844; All Open Access, Hybrid Gold Open Access, 2020.
- Holton, J. R. and Gettelman, A.: Horizontal transport and the dehydration of the stratosphere, Geophysical Research Letters, 28, 2799 2802, https://doi.org/10.1029/2001GL013148, cited by: 318, 2001.
  - Homeyer, C. R., Smith, J. B., Bedka, K. M., Bowman, K. P., Wilmouth, D. M., Ueyama, R., Dean-Day, J. M., St. Clair, J. M., Hannun, R., Hare, J., et al.: Extreme altitudes of stratospheric hydration by midlatitude convection observed during the DCOTSS field campaign, Geophysical Research Letters, 50, e2023GL104 914, 2023.
- Homeyer, C. R., Gordon, A. E., Smith, J. B., Ueyama, R., Wilmouth, D. M., Sayres, D. S., Hare, J., Pandey, A., Hanisco, T. F., Dean-Day, J. M., et al.: Stratospheric hydration processes in tropopause-overshooting convection revealed by tracer-tracer correlations from the DCOTSS field campaign, Journal of Geophysical Research: Atmospheres, 129, e2024JD041 340, 2024.
  - Honomichl, S. B. and Pan, L. L.: Transport From the Asian Summer Monsoon Anticyclone Over the Western Pacific, Journal of Geophysical Research: Atmospheres, 125, https://doi.org/10.1029/2019JD032094, cited by: 27, 2020.
- 695 Jensen, E., Pan, L., Honomichl, S., Diskin, G., Krämer, M., Spelten, N., Günther, G., Hurst, D., Fujiwara, M., Vömel, H., Selkirk, H., Suzuki, J., Schwartz, M., and Smith, J.: Assessment of Observational Evidence for Direct Convective Hydration of the Lower Stratosphere, Journal of Geophysical Research: Atmospheres, 125, https://doi.org/10.1029/2020JD032793, cited By 20, 2020.
  - Jorgensen, D. and Lemone, M.: Vertical velocity characteristics of oceanic convection, Journal of the Atmospheric Sciences, 46, 621 640, https://doi.org/10.1175/1520-0469(1989)046<0621:VVCOOC>2.0.CO;2, cited by: 201; All Open Access, Bronze Open Access, 1989.
- Konopka, P., Tao, M., Von Hobe, M., Hoffmann, L., Kloss, C., Ravegnani, F., Volk, C. M., Lauther, V., Zahn, A., Hoor, P., and Ploeger, F.: Tropospheric transport and unresolved convection: numerical experiments with CLaMS 2.0/MESSy, Geoscientific Model Development, 15, 7471 7487, https://doi.org/10.5194/gmd-15-7471-2022, cited by: 5; All Open Access, Gold Open Access, Green Open Access, 2022.

705

- Konopka, P., Rolf, C., Von Hobe, M., Khaykin, S. M., Clouser, B., Moyer, E., Ravegnani, F., D'Amato, F., Viciani, S., Spelten, N., Afchine, A., Krämer, M., Stroh, F., and Ploeger, F.: The dehydration carousel of stratospheric water vapor in the Asian summer monsoon anticyclone, Atmospheric Chemistry and Physics, 23, 12 935 12 947, https://doi.org/10.5194/acp-23-12935-2023, cited by: 0, 2023.
- Kumar, V. and Krishnan, R.: On the association between the Indian summer monsoon and the tropical cyclone activity over northwest Pacific, Current science, pp. 602–612, 2005.
- Lambert, A., Werner, F., Read, W. G., Froidevaux, L., Schwartz, M. J., Wagner, P. A., Daffer, W. H., Livesey, N. J., Pumphrey, H. C., Manney, G. L., et al.: Version 5 Level-2 Near-Real-Time Data User Guide, Tech. rep., Tech. Rep. JPL D-48439 d, Jet Propulsion Laboratory, California Institute of ..., 2017.
- Liu, C., Zipser, E. J., and Nesbitt, S. W.: Global distribution of tropical deep convection: Different perspectives from TRMM infrared and radar data, Journal of Climate, 20, 489 503, https://doi.org/10.1175/JCLI4023.1, cited by: 190; All Open Access, Bronze Open Access, Green Open Access, 2007.

- Liu, Y., Fueglistaler, S., and Haynes, P.: Advection-condensation paradigm for stratospheric water vapor, Journal of Geophysical Research
  Atmospheres, 115, https://doi.org/10.1029/2010JD014352, cited by: 62, 2010.
  - Livesey, N., Read, W., Wagner, L., Froidevaux, P., Lambert, A., Manney, G., Millán Valle, L., Pumphrey, H., Santee, M., Schwartz, M., et al.: Version 4.2 x Level 2 and 3 data quality and description document (Tech. Rep. No. JPL D-33509 Rev. E), Jet Propulsion Laboratory, 2020.
- McKenna, D. S., Grooß, J.-U., Günther, G., Konopka, P., Müller, R., Carver, G., and Sasano, Y.: A new Chemical Lagrangian Model of the

  Stratosphere (CLaMS) 2. Formulation of chemistry scheme and initialization, Journal of Geophysical Research Atmospheres, 107, ACH

  4–1 ACH 4–14, https://doi.org/10.1029/2000JD000113, cited by: 116, 2002.
  - Mote, P. W., Rosenlof, K. H., Holton, J. R., Harwood, R. S., and Waters, J. W.: Seasonal variations of water vapor in the tropical lower stratosphere, Geophysical Research Letters, 22, 1093 1096, https://doi.org/10.1029/95GL01234, cited by: 83, 1995.
- Mote, P. W., Rosenlof, K. H., McIntyre, M. E., Carr, E. S., Gille, J. C., Holton, J. R., Kinnersley, J. S., Pumphrey, H. C., Russell III, J. M.,
   and Waters, J. W.: An atmospheric tape recorder: The imprint of tropical tropopause temperatures on stratospheric water vapor, Journal of Geophysical Research Atmospheres, 101, 3989 4006, https://doi.org/10.1029/95JD03422, cited by: 626; All Open Access, Green Open Access, 1996.
  - Nützel, M., Podglajen, A., Garny, H., and Ploeger, F.: Quantification of water vapour transport from the Asian monsoon to the stratosphere, Atmospheric Chemistry and Physics, 19, 8947 8966, https://doi.org/10.5194/acp-19-8947-2019, cited by: 22; All Open Access, Gold Open Access, 2019.

## Pan, L.

730

- O'Neill, M., Orf, L., Honomichl, S. B., Bui, T. V., Thornberry, T., Rollins Heymsfield, G., and Halbert, K.: Hydraulic jump dynamics above supercell thunderstorms, Science, 373, 1248–1251, https://doi.org/10.1126/science.abh3857, cited By 24, 2021.
- Park, M., Randel, W. J., Gettelman, A., Hintsa, EMassie, S. T., and Jensen, E. J.: Lapse rate or cold point: The tropical tropopause identified by in situ trace gas measurements, Geophysical Research Letters, 45, 10–756, 2018. Jiang, J. H.: Transport above the Asian summer monsoon anticyclone inferred from Aura Microwave Limb Sounder tracers, Journal of Geophysical Research Atmospheres, 112, https://doi.org/10.1029/2006JD008294, cited by: 280; All Open Access, Bronze Open Access, Green Open Access, 2007.
  - Park, M., Randel, W. J., Damadeo, R. P., Flittner, D. E., Davis, S. M., Rosenlof, K. H., Livesey, N., Lambert, A., and Read, W.: Near-Global Variability of Stratospheric Water Vapor Observed by SAGE III/ISS, Journal of Geophysical Research: Atmospheres, 126, https://doi.org/10.1029/2020JD034274, cited by: 6; All Open Access, Green Open Access, 2021.
  - Peña-Ortiz, C., Plaza, N. P., Gallego, D., and Ploeger, F.: Quasi-biennial oscillation modulation of stratospheric water vapour in the Asian monsoon, Atmospheric Chemistry and Physics, 24, 5457 5478, https://doi.org/10.5194/acp-24-5457-2024, cited by: 0, 2024.
  - Pisso, I., Marécal, V., Legras, B., and Berthet, G.: Sensitivity of ensemble Lagrangian reconstructions to assimilated wind time step resolution, Atmospheric Chemistry and Physics, 10, 3155–3162, https://doi.org/10.5194/acp-10-3155-2010, cited By 11, 2010.
- Plaza, N. P., Podglajen, A., Peña-Ortiz, C., and Ploeger, F.: Processes influencing lower stratospheric water vapour in monsoon anticyclones: insights from Lagrangian modelling, Atmospheric Chemistry and Physics, 21, 9585–9607, 2021.
  - Ploeger, F., Fueglistaler, S., Grooß, J.-U., Günther, G., Konopka, P., Liu, Y., Uller, R., Ravegnani, F., Schiller, C., Ulanovski, A., and Riese, M.: Insight from ozone and water vapour on transport in the tropical tropopause layer (TTL), Atmospheric Chemistry and Physics, 11, 407–419, https://doi.org/10.5194/acp-11-407-2011, cited By 54, 2011.

Ploeger, F., Günther, G., Konopka, P., Fueglistaler, S., Müller, R., Hoppe, C., Kunz, A., Spang, R., Grooß, J.-U., and Riese, M.: Horizontal water vapor transport in the lower stratosphere from subtropics to high latitudes during boreal summer, Journal of Geophysical Research Atmospheres, 118, 8111 – 8127, https://doi.org/10.1002/jgrd.50636, cited by: 98; All Open Access, Green Open Access, 2013.

755

760

765

770

780

- Poshyvailo, L., Müller, R., Konopka, P., Günther, G., Riese, M., Podglajen, A., and Ploeger, F.: Sensitivities of modelled water vapour in the lower stratosphere: Temperature uncertainty, effects of horizontal transport and small-scale mixing, Atmospheric Chemistry and Physics, 18, 8505–8527, https://doi.org/10.5194/acp-18-8505-2018, cited By 18, 2018.
- Randel, W. and Park, M.: Diagnosing Observed Stratospheric Water Vapor Relationships to the Cold Point Tropical Tropopause, Journal of Geophysical Research: Atmospheres, 124, 7018–7033, https://doi.org/10.1029/2019JD030648, cited By 50, 2019.
- Randel, W., Moyer, E., Park, M., Jensen, E., Bernath, P., Walker, K., and Boone, C.: Global variations of HDO and HDO/H2O ratios in the upper troposphere and lower stratosphere derived from ACE-FTS satellite measurements, Journal of Geophysical Research Atmospheres, 117, https://doi.org/10.1029/2011JD016632, cited By 69, 2012.
- Randel, W. J., Wu, F., Oltmans, S. J., Rosenlof, K., and Nedoluha, G. E.: Interannual changes of stratospheric water vapor and correlations with tropical tropopause temperatures, Journal of the Atmospheric Sciences, 61, 2133 2148, https://doi.org/10.1175/1520-0469(2004)061<2133:ICOSWV>2.0.CO;2, cited by: 216; All Open Access, Bronze Open Access, 2004.
- Randel, W. J., Zhang, K., and Fu, R.: What controls stratospheric water vapor in the NH summer monsoon regions?, JOURNAL OF GEO-PHYSICAL RESEARCH-ATMOSPHERES, 120, 7988–8001, https://doi.org/10.1002/2015JD023622, 2015.
- Read, W., Lambert, A., Bacmeister, J., Cofield, R., Christensen, L., Cuddy, D., Daffer, W., Drouin, B., Fetzer, E., Froidevaux, L., Fuller, R., Herman, R., Jarnot, R., Jiang, J., Jiang, Y., Kelly, K., Knosp, B., Kovalenko, L., Livesey, N., Liu, H.-C., Manney, G., Pickett, H., Pumphrey, H., Rosenlof, K. H., Sabounchi, X., Santee, M., Schwartz, M., Snyder, W., Stek, P., Su, H., Takacs, L., Thurstans, R., Vömel, H., Wagner, P., Waters, J., Webster, C., Weinstock, E., and Wu, D.: Aura Microwave Limb Sounder upper tropospheric and lower stratospheric H2O and relative humidity with respect to ice validation, Journal of Geophysical Research Atmospheres, 112,
- Riese, M., Ploeger, F., Rap, A., Vogel, B., Konopka, P., Dameris, M., and Forster, P.: Impact of uncertainties in atmospheric mixing on simulated UTLS composition and related radiative effects, JOURNAL OF GEOPHYSICAL RESEARCH-ATMOSPHERES, 117, https://doi.org/10.1029/2012JD017751, 2012.
- Rolf, C., Vogel, B., Hoor, P., Afchine, A., Günther, G., Krämer, M., Müller, R., Müller, S., Spelten, N., and Riese, M.: Water vapor increase in the lower stratosphere of the Northern Hemisphere due to the Asian monsoon anticyclone observed during the TACTS/ESMVal campaigns, Atmospheric Chemistry and Physics, 18, 2973 2983, https://doi.org/10.5194/acp-18-2973-2018, cited by: 23; All Open Access, Gold Open Access, 2018.

https://doi.org/10.1029/2007JD008752, cited by: 193; All Open Access, Bronze Open Access, 2007.

- Schiller, C., Groob, J.-U., Konopka, P., Plöger, F., Silva Dos Santos, F., and Spelten, N.: Hydration and dehydration at the tropical tropopause, Atmospheric Chemistry and Physics, 9, 9647–9660, https://doi.org/10.5194/acp-9-9647-2009, cited By 73, 2009.
- Schoeberl, M. and Dessler, A.: Dehydration of the stratosphere, Atmospheric Chemistry and Physics, 11, 8433 8446, https://doi.org/10.5194/acp-11-8433-2011, cited by: 92; All Open Access, Gold Open Access, Green Open Access, 2011.
- Schoeberl, M. R., Dessler, A. E., and Wang, T.: Modeling upper tropospheric and lower stratospheric water vapor anomalies, Atmospheric Chemistry and Physics, 13, 7783–7793, https://doi.org/10.5194/acp-13-7783-2013, 2013.
- Schwartz, M. J., Read, W. G., Santee, M. L., Livesey, N. J., Froidevaux, L., Lambert, A., and Manney, G. L.: Convectively injected water vapor in the North American summer lowermost stratosphere, Geophysical Research Letters, 40, 2316 2321, https://doi.org/10.1002/grl.50421, cited by: 70; All Open Access, Bronze Open Access, 2013.

- Smith, J., Wilmouth, D., Bedka, K., Bowman, K., Homeyer, C., Dykema, J., Sargent, M., Clapp, C., Leroy, S., Sayres, D., Dean-Day, J.,
  Paul Bui, T., and Anderson, J.: A case study of convectively sourced water vapor observed in the overworld stratosphere over the United

  States, Journal of Geophysical Research: Atmospheres, 122, 9529–9554, https://doi.org/10.1002/2017JD026831, cited By 64, 2017.
  - Smith, J., Haynes, P., Maycock, A., Butchart, N., and Bushell, A.: Sensitivity of stratospheric water vapour to variability in tropical tropopause temperatures and large-scale transport, Atmospheric Chemistry and Physics, 21, 2469–2489, https://doi.org/10.5194/acp-21-2469-2021, cited By 7, 2021.
- Solomon, S., Rosenlof, K. H., Portmann, R. W., Daniel, J. S., Davis, S. M., Sanford, T. J., and Plattner, G.-K.: Contributions of Stratospheric Water Vapor to Decadal Changes in the Rate of Global Warming, SCIENCE, 327, 1219–1223, https://doi.org/10.1126/science.1182488, 2010.
  - $Sonntag, D.: Advancements in the field of hygrometry, Meteorologische Zeitschrift, 3, 51–66, \\https://doi.org/10.1127/metz/3/1994/51, 1994.$
  - Tao, M., Konopka, P., Wright, J. S., Liu, Y., Bian, J., Davis, S. M., Jia, Y., and Ploeger, F.: Multi-decadal variability controls short-term stratospheric water vapor trends, Communications Earth and Environment, 4, https://doi.org/10.1038/s43247-023-01094-9, cited by: 2; All Open Access, Gold Open Access, 2023.

- Tegtmeier, S., Anstey, J., Davis, S., Dragani, R., Harada, Y., Ivanciu, I., Pilch Kedzierski, R., Krüger, K., Legras, B., Long, C., Wang, J. S., Wargan, K., and Wright, J. S.: Temperature and tropopause characteristics from reanalyses data in the tropical tropopause layer, Atmospheric Chemistry and Physics, 20, 753–770, , 2020.
- Ueyama, R., Jensen, E., Pfister, L., Krämer, M., Afchine, A., and Schoeberl, M.: Impact of Convectively Detrained Ice Crystals on the Humidity of the Tropical Tropopause Layer in Boreal Winter, Journal of Geophysical Research: Atmospheres, 125, https://doi.org/10.1029/2020JD032894, cited By 9, 2020.
  - Ueyama, R., Schoeberl, M., Jensen, E., Pfister, L., Park, M., and Ryoo, J.-M.: Convective Impact on the Global Lower Stratospheric Water Vapor Budget, Journal of Geophysical Research: Atmospheres, 128, https://doi.org/10.1029/2022JD037135, cited By 8, 2023.
- Vogel, B., Müller, R., Günther, G., Spang, R., Hanumanthu, S., Li, D., Riese, M., and Stiller, G.: Lagrangian simulations of the transport of young air masses to the top of the Asian monsoon anticyclone and into the tropical pipe, Atmospheric Chemistry and Physics, 19, 6007–6034, https://doi.org/10.5194/acp-19-6007-2019, cited By 64, 2019.
  - Waters, J. W., Froidevaux, L., Harwood, R. S., Jarnot, R. F., Pickett, H. M., Read, W. G., Siegel, P. H., Cofield, R. E., Filipiak, M. J., Flower, D. A., et al.: The earth observing system microwave limb sounder (EOS MLS) on the Aura satellite, IEEE transactions on geoscience and remote sensing, 44, 1075–1092, 2006.
- Wright, C. and Gille, J.: HIRDLS observations of gravity wave momentum fluxes over the monsoon regions, Journal of Geophysical Research Atmospheres, 116, https://doi.org/10.1029/2011JD015725, cited by: 35, 2011.
  - Yu, W., Dessler, A. E., Park, M., and Jensen, E. J.: Influence of convection on stratospheric water vapor in the North American monsoon region, Atmospheric Chemistry and Physics, 20, 12153 12161, https://doi.org/10.5194/acp-20-12153-2020, cited by: 12; All Open Access, Gold Open Access, Green Open Access, 2020.